A Comparison of Two Cumulus Parameterization Schemes in a Linear Model a Wave-Cisk

by
Francis X. Crum and Duane E. Stevens

Department of Atmospheric Science
Colorado State University
Fort Collins, Colorado

Colorado State University

Department of Atmospheric Science

Paper No. 353

A COMPARISON OF TWO CUMULUS PARAMETERIZATION SCHEMES IN A LINEAR MODEL OF WAVE-CISK

by

Francis X. Crum
and
Duane E. Stevens

Research supported by the
Office of Naval Research and
the National Science Foundation
under grants
N00014-79-C-0793 and ATM-8107136

Department of Atmospheric Science
Colorado State University
Fort Collins, Colorado

August, 1982

Atmospheric Science Paper No. 353

ABSTRACT

A model of wave-CISK consisting of the primitive equations formulated on an equatorial beta-plane with a resting basic state is used to compare the relatively simple cumulus parameterization scheme developed by Stevens and Lindzen (1978) with the relatively complex one developed by Arakawa and Schubert (1974). The comparison is based mainly on the instability characteristics and vertical structure of the wave.

Discrete forms of the equations are developed and the inhomogeneous vertical structure equation is solved as a generalized matrix eigenvalue problem. The eigenvalues are equivalent depths which are used with the dispersion relation for an equatorial beta plane to find growth rates.

Results indicate that the growth rates obtained with Arakawa and Schubert parameterization are smaller than those obtained with Stevens and Lindzen parameterization. It is concluded that, although there is some qualitative similarity between the two parameterizations, there are notable quantitative differences.

ACKNOWLEDGEMENTS

We have benefited from discussions with Dr. Wayne Schubert, Dr. Richard Johnson, Mr. Melville Nicholls, Mr. Scott Fulton, Mr. Mark DeMaria and Mr. Timothy Stoker. Special thanks are extended to Ms. Machel Sandfort for her skillful use of the word processor in preparation of this thesis and to Ms. Judy Sorbie for drafting the figures.

This research was sponsored by the Office of Naval Research, Grant N00014-79-C-0793 and by the National Science Foundation, Grant ATM-8107136.

TABLE OF CONTENTS

		Page
	ABSTRACT	ii
	ACKNOWLEDGEMENTS	iii
	TABLE OF CONTENTS	iv
	LIST OF TABLES	vi
	LIST OF FIGURES	vii
1.	INTRODUCTION	1
2.	LARGE-SCALE GOVERNING EQUATIONS	4
	2.1 Linearization and Fourier Series Expansion	4
	2.2 Derivation of the Vertical Structure Equation and the Dispersion Relation	8
3.	CUMULUS PARAMETERIZATION	14
	3.1 Stevens and Lindzen Parameterization	14
	3.2 Arakawa and Schubert Parameterization	17
4.	DISCRETE FORMS AND SOLUTION TECHNIQUE	24
	4.1 The Vertical Structure Problem	24
	4.2 Cumulus Parameterization	27
5.	RESULTS	35
6.	SUMMARY AND CONCLUSIONS	64

TABLE OF CONTENTS (continued)

		Page
REFERENCES		67
APPENDIX A:	PRINCIPAL SYMBOLS	69
APPENDIX B:	DETERMINATION OF THE SATURATION MIXING RATIO AND GAMMA	72
APPENDIX C:	THE DISCRETE FORM OF THE FREDHOLM INTEGRAL EQUATION	73

LIST OF TABLES

TABLE		PAGE
5.1	Phase speeds $\sqrt{gh}$ obtained from the homogeneous vertical structure problem for $\Gamma = 23.79°K$ = constant and for Γ given by Fig. 5.2. Units are m/s.....	38
5.2	Fractional entrainment rate $\tilde{\lambda}$ and detrainment pressure $\hat{p}$ for each cloud type.....	50

LIST OF FIGURES

FIGURE		PAGE
4.1	Vertical grid used in the model.....	25
5.1	Profiles of basic state temperature $\bar{T}$ (solid line) and basic state mixing ratio $\bar{q}$ (dashed line).....	36
5.2	The static stability Γ calculated from the basic state temperature profile of Fig. 5.1.....	37
5.3	Eigenvectors W for n = 0, 1, 2, 3, as labeled for (a) constant static stability $\Gamma = 23.79°K$ and (b) the static stability of Fig. 5.2.....	39
5.4	Mixing ratio $\bar{q}$ calculated from (3.8) for $p_a = 880$ mb, $p_d = 200$ mb, $q_a = 16$ g/kg and (a) $\delta = 0.5\times10^{-2}mb^{-1}$, (b) $\delta = 1.0\times10^{-2}mb^{-1}$, (c) $\delta = 2.0\times10^{-2}mb^{-1}$.....	41
5.5	Eigenvalues gh as a function of q_a for $p_a=p_d=795$ mb and $\delta = \infty$.....	42
5.6	The e-folding times and phase speeds as a function of q_a for the two most unstable modes of Fig. 5.5 computed for a gravity wave of wavelength 300 km and meridional mode n = 1.....	44
5.7	Amplitude and phase of (a) the vertical velocity and (b) the adiabatic cooling (solid line) and cumulus heating (dashed line) for the most unstable mode in Fig. 5.6 at $q_a = 12$ g/kg.....	45
5.8	Eigenvalues gh as a function of δ for $p_a = 880$ mb, $p_d = 200$ mb and $q_a = 16$ g/kg.....	47
5.9	Vertical profiles of $\bar{h}$, $\bar{h}^*$ and $\bar{h}_c$. Lines of $\bar{h}_c$ are dashed and each line corresponds to one of the nine cloud types present in the model.....	48
5.10	Vertical profile of the normalized mass flux $\bar{\eta}$ for each cloud type.....	49

FIGURE		PAGE
5.11	Autoconversion coefficient c_0 calculated from (5.1) for a = 90 mb, c = 450 mb and (a) b = 3 km^{-1}, (b) b = 5 km^{-1} and (c) b = 6 km^{-1}.....	51
5.12	Eigenvalues gh as a function of c_0 for the case where c_0 is constant and independent of cloud type.....	53
5.13	Eigenvalues gh as a function of b.....	54
5.14	The e-folding times and phase speeds as a function of c_0 for the unstable modes in Fig. 5.12 computed for a gravity wave of wavelength 300 km and meridional mode n = 1.....	56
5.15	The e-folding times and phase speeds as a function of b for the unstable modes in Fig. 5.13 computed for a gravity wave of wavelength 300 km and meridional mode n = 1.....	57
5.16	Amplitude and phase of (a) the vertical velocity and (b) the adiabatic cooling (solid line) and cumulus heating (dashed line) for the most unstable mode in Fig. 5.15 at b = 5 km^{-1}.....	58
5.17	Amplitude and phase of (a) the vertical velocity and (b) the adiabatic cooling (solid line) and cumulus heating (dashed line) for the most unstable mode in Fig. 5.14 at c_0 = 2 km^{-1}.....	59
5.18	Same as Fig. 5.17 except for c_0 = 4 km^{-1}.....	60
5.19	The magnitude of the phase speed as a function of wavelength for several meridional modes n and for all wave types possible on an equatorial beta-plane. Here gh = 146.3 + 27.3i m^2/s^2.....	62
5.20	Same as Fig. 5.19 except for the magnitude of the e-folding time as a function of wavelength.....	63

1. INTRODUCTION

The interaction of cumulus clouds with a large-scale atmospheric disturbance is one of the fundamental problems in the study of the dynamics of the tropical atmosphere. In the classical papers of Charney and Eliassen (1964) and Ooyama (1964), the mechanism of CISK (Conditional Instability of the Second Kind) was proposed to explain this interaction. In this mechanism, it is postulated that large-scale convergence results in the formation of cumulus clouds which, due to the release of latent heat, modify the large-scale environment in such a way as to increase the large-scale convergence and correspondingly increase the amount of latent heat released. The instability results from the feedback from the cumulus-scale to the large-scale. In the original formulation of the CISK mechanism the large-scale convergence was frictionally induced. In wave-CISK (Hayashi, 1970; Lindzen, 1974), the large-scale convergence is assumed to be the convergence which is naturally associated with an atmospheric wave such as a gravity wave or Rossby wave.

The central element in any mathematical model of the wave-CISK mechanism is the cumulus parameterization, i.e., the method by which the release of latent heat by cumulus clouds is related to the large-scale flow. Many different techniques of cumulus parameterization have been proposed in previous studies of wave-CISK. Hayashi (1970) related the latent heat release to the large-scale vertical velocity at cloud base

and arbitrarily specified both the magnitude of the heating and its vertical profile. Lindzen (1974) related the heating to the large-scale vertical velocity at the top of the mixed layer, and also arbitrarily specified both its magnitude and its vertical profile. Kuo (1975) related the heating to the large-scale vertical velocity at the top of the moist layer, specified its magnitude and let its vertical profile be determined by the temperature difference between deep cumulus clouds and the environment. An improvement to these schemes was made by Stevens and Lindzen (1978). In their study, the heating was related to the large-scale vertical velocity at the top of the moist layer through on explicit moisture budget constraint, and, although the vertical profile of the heating was arbitrarily specified, its magnitude was determined from the moisture budget. Stark (1976) used a simplified version of the parameterization developed by Arakawa and Schubert (1974). With this parameterization, the heating was related to the large-scale vertical velocity at every level in the vertical and both the magnitude and vertical profile of the heating were determined from the large-scale. A similar analysis was also performed by Wada (1977).

In this research a model of the wave-CISK mechanism is developed in order to compare the relatively simple parameterization scheme developed by Stevens and Lindzen with the relatively complex one developed by Arakawa and Schubert. The comparison is based mainly on the instability characteristics and vertical structure of the wave. The model consists of the linearized, primitive equations formulated on an equatorial beta-plane with a resting basic state. In Chapter 2 the large-scale governing equations are presented. Here the vertical structure equation and its boundary conditions are derived along with the disperion

relation which governs waves on an equatorial beta-plane. Chapter 3 contains the governing equations for both parameterization schemes. The vertically discrete forms of the governing equations for both the large-scale and the parameterizations are presented in Chapter 4 where it is shown that the vertical structure equation, which includes the effects of latent heat release, can be solved as a generalized matrix eigenvalue problem. The eigenvalues are equivalent depths, which are used with the dispersion relation for an equatorial beta-plane to find growth rates. Results are presented in Chapter 5. Chapter 6 contains a summary and conclusions.

2. LARGE-SCALE GOVERNING EQUATIONS

This chapter presents the governing equations for the large-scale motion. In section 2.1 these equations are linearized. Each of the dependent variables and the diabatic heating are then expanded in a Fourier series and it is shown that the linearized equations are valid term-by-term for every term in each of the expansions. The vertical structure equation and its boundary conditions are derived in section 2.2 along with the dispersion relation for an equatorial beta-plane.

2.1 Linearization and Fourier Series Expansion

The governing equations for the large-scale motion are the horizontal momentum equations, the mass continuity equation and the thermodynamic energy equation. We also consider the atmosphere to be in hydrostatic balance. These equations, formulated in p-coordinates on an equatorial beta-plane ($f = \beta y$), may be written as

$$\frac{du}{dt} - fv + \frac{\partial \phi}{\partial x} = 0, \tag{2.1a}$$

$$\frac{dv}{dt} + fu + \frac{\partial \phi}{\partial y} = 0, \tag{2.1b}$$

$$\frac{\partial \phi}{\partial p} + \frac{RT}{p} = 0, \tag{2.1c}$$

$$\frac{\partial u}{\partial x} + \frac{\partial v}{\partial y} + \frac{\partial \omega}{\partial p} = 0, \tag{2.1d}$$

$$\frac{dT}{dt} - \frac{RT}{pc_p}\omega = \frac{Q}{c_p}. \tag{2.1e}$$

Here t is time, x and y are the horizontal positions, p is pressure, $u = dx/dt$ and $v = dy/dt$ are the horizontal velocity components, $\omega = dp/dt$ is the "vertical velocity" in p-coordinates, ϕ is the geopotential, T is the temperature, f is the coriolis parameter, R is the gas constant for dry air, c_p is the specific heat at constant pressure for dry air, Q is the diabatic heating and

$$\frac{d}{dt} = \frac{\partial}{\partial t} + u \frac{\partial}{\partial x} + v \frac{\partial}{\partial y} + \omega \frac{\partial}{\partial p} \tag{2.2}$$

is the time derivative following the motion. Symbols are also defined in Appendix A.

We linearize these equations about the basic state defined below. Letting basic state quantities be denoted by overbars we have

$$\left.\begin{aligned} \bar{u} &= 0, \\ \bar{v} &= 0, \\ \bar{\omega} &= 0, \\ \bar{\phi} &= \bar{\phi}(p), \\ \bar{T} &= \bar{T}(p), \end{aligned}\right\} \tag{2.3}$$

where $\bar{\phi}$ and $\bar{T}$ are specified. Requiring that the basic state satisfy the system (2.1) leads to

$$\frac{d\bar{\phi}}{dp} + \frac{R\bar{T}}{p} = 0 \tag{2.4}$$

and the fact that the mean diabatic heating $\bar{Q}$ must be zero.

Now we express each of the dependent variables in (2.1) and the diabatic heating Q as the sum of a basic state part given by (2.3) and a

perturbation from that basic state. Denoting the perturbations by primes we have

$$\left.\begin{aligned} u(x,y,p,t) &= u'(x,y,p,t), \\ v(x,y,p,t) &= v'(x,y,p,t), \\ \omega(x,y,p,t) &= \omega'(x,y,p,t), \\ \phi(x,y,p,t) &= \bar{\phi}(p) + \phi'(x,y,p,t), \\ T(x,y,p,t) &= \bar{T}(p) + T'(x,y,p,t), \\ Q(x,y,p,t) &= Q'(x,y,p,t). \end{aligned}\right\} \tag{2.5}$$

Substituting (2.5) into (2.1), using (2.2) and (2.4), and neglecting the products of perturbation quantities we obtain the system of linearized equations

$$\frac{\partial u'}{\partial t} - fv' + \frac{\partial \phi'}{\partial x} = 0, \tag{2.6a}$$

$$\frac{\partial v'}{\partial t} + fu' + \frac{\partial \phi'}{\partial y} = 0, \tag{2.6b}$$

$$\frac{\partial \phi'}{\partial p} + \frac{RT'}{p} = 0, \tag{2.6c}$$

$$\frac{\partial u'}{\partial x} + \frac{\partial v'}{\partial y} + \frac{\partial \omega'}{\partial p} = 0, \tag{2.6d}$$

$$\frac{\partial T'}{\partial t} + \left(\frac{d\bar{T}}{dp} - \frac{R\bar{T}}{pc_p}\right)\omega' = \frac{Q'}{c_p}. \tag{2.6e}$$

Now the assumption is made that each of the dependent variables is periodic in x with period L and is sufficiently smooth so that convergence is assured not only for the Fourier series expansion of each variable but also for the series obtained by term-by-term integration or differentiation of the Fourier series. If we further assume that each dependent variable has a time dependence given by $e^{-i\sigma t}$ where σ depends on the summation index of the Fourier series and may be complex,

and that these assumptions also apply for the diabatic heating Q, then we may write

$$\left.\begin{aligned}
u'(x,y,p,t) &= \sum_{n=-\infty}^{\infty} u(n,y,p)e^{i(\frac{2n\pi}{L}x-\sigma(n)t)}, \\
v'(x,y,p,t) &= \sum_{n=-\infty}^{\infty} v(n,y,p)e^{i(\frac{2n\pi}{L}x-\sigma(n)t)}, \\
\omega'(x,y,p,t) &= \sum_{n=-\infty}^{\infty} \omega(n,y,p)e^{i(\frac{2n\pi}{L}x-\sigma(n)t)}, \\
\phi'(x,y,p,t) &= \sum_{n=-\infty}^{\infty} \phi(n,y,p)e^{i(\frac{2n\pi}{L}x-\sigma(n)t)}, \\
T'(x,y,p,t) &= \sum_{n=-\infty}^{\infty} T(n,y,p)e^{i(\frac{2n\pi}{L}x-\sigma(n)t)}, \\
Q'(x,y,p,t) &= \sum_{n=-\infty}^{\infty} Q(n,y,p)e^{i(\frac{2n\pi}{L}x-\sigma(n)t)}.
\end{aligned}\right\} \qquad (2.7)$$

Because the perturbation quantities are real, it may be shown that the coefficient in each expansion with index n=-m must be the complex conjugate of the coefficient with index n=m and furthermore, that σ must depend on n such that $Re\{\sigma(n)\} = -Re\{\sigma(-n)\}$. Substituting (2.7) into (2.6), multiplying by $e^{-i\frac{2n\pi}{L}x}$, integrating from -L/2 to L/2, using the orthogonality properties of complex exponentials, dropping the notation referring to the n dependence of σ, and defining $k = 2n\pi/L$ we find

$$-i\sigma u - fv + ik\phi = 0, \tag{2.8a}$$

$$-i\sigma v + fu + \frac{\partial \phi}{\partial y} = 0, \tag{2.8b}$$

$$\frac{\partial \phi}{\partial p} + \frac{RT}{p} = 0, \tag{2.8c}$$

$$iku + \frac{\partial v}{\partial y} + \frac{\partial \omega}{\partial p} = 0, \tag{2.8d}$$

$$-i\sigma T + (\frac{d\bar{T}}{dp} - \frac{R\bar{T}}{pc_p})\omega = \frac{Q}{c_p}. \tag{2.8e}$$

Note that the system (2.8) is the same system we would obtain if we evaluated (2.6) for any one term in the Fourier expansions. This result is due to the fact that (2.6) is a linear system with coefficients that are independent of x. The derivation of the vertical structure equation and the dispersion relation proceeds from the system (2.8).

2.2 Derivation of the Vertical Structure Equation and the Dispersion Relation

The system (2.8) may be reduced to a single equation for ω as follows. Eliminating u from (2.8a) and (2.8b) yields

$$(\sigma^2 - f^2)v + (i\sigma \frac{\partial}{\partial y} + ikf)\phi = 0. \tag{2.9}$$

Eliminating u from (2.8a) and (2.8d) gives

$$(\sigma \frac{\partial}{\partial y} - fk)v + ik^2\phi + \sigma \frac{\partial \omega}{\partial p} = 0. \tag{2.10}$$

Now we eliminate v from (2.9) and (2.10) to obtain

$$L_y\phi = -\frac{1}{i\sigma}(f^2 - \sigma^2)\frac{\partial \omega}{\partial p}, \tag{2.11}$$

where L_y is a y-operator defined by

$$L_y = \frac{\partial^2}{\partial y^2} - \frac{2f\beta}{f^2-\sigma^2}\frac{\partial}{\partial y} + (\frac{k\beta}{\sigma} - \frac{2\beta k f^2}{\sigma(\sigma^2-f^2)} - k^2). \tag{2.12}$$

Eliminating T from (2.8c) and (2.8e) yields

$$i\sigma \frac{\partial \phi}{\partial p} - S\omega = \frac{\kappa}{p} Q, \tag{2.13}$$

where S is a measure of the static stability and is given by

$$S = -\frac{R}{p} \left(\frac{d\bar{T}}{dp} - \frac{R\bar{T}}{pc_p}\right). \tag{2.14}$$

Finally, we operate on (2.13) with L_y and use (2.11) to obtain

$$-(f^2-\sigma^2) \frac{\partial^2 \omega}{\partial p^2} - SL_y\omega = \frac{\kappa}{p} L_y Q. \tag{2.15}$$

This single equation for ω may be solved by separation of variables. We write

$$\omega(y,p) = W(p)Y(y) \tag{2.16}$$

and

$$Q(y,p) = J(p)Y(y), \tag{2.17}$$

Here we have assumed that ω and Q have the same y-structure. This assumption is justified by the fact that the governing equations for both Stevens and Lindzen parameterization and Arakawa and Schubert parameterization (see chapter 3) involve no y-derivatives. Furthermore, it may be shown that (2.15) is not separable unless the y-structures are the same. Upon substituting (2.16) and (2.17) into (2.15) we find

$$\frac{\frac{d^2W}{dp^2}}{\frac{\kappa J}{p} + SW} = \frac{-L_y Y}{(f^2-\sigma^2)Y} = -\frac{1}{gh}, \tag{2.18}$$

where -1/gh is the separation constant and g is the acceleration of gravity. The vertical structure equation is then

$$\frac{d^2W}{dp^2} + \frac{S}{gh} W = \frac{-\kappa J}{ghp} \tag{2.19}$$

and the horizontal structure equation is

$$L_y Y - \frac{f^2-\sigma^2}{gh} Y = 0. \tag{2.20}$$

Using (2.16) and (2.17) it may be shown from (2.13) that ϕ and ω have the same y-structure. If we use this fact to combine (2.11) and (2.20) we find

$$-i\sigma\phi - gh \frac{\partial \omega}{\partial p} = 0, \tag{2.21}$$

or, upon substituting from (2.8d),

$$-i\sigma\phi + gh \left(iku + \frac{\partial v}{\partial y}\right) = 0. \tag{2.22}$$

Rewriting this equation together with (2.8a) and (2.8b) we have

$$-i\sigma u - fv + ik\phi = 0, \tag{2.23a}$$

$$-i\sigma v + fu + \frac{\partial \phi}{\partial y} = 0, \tag{2.23b}$$

$$-i\sigma\phi + gh \left(iku + \frac{\partial v}{\partial y}\right) = 0. \tag{2.23c}$$

This system is formally the same as the system obtained by linearizing the shallow water equations and assuming solutions in the form of a Fourier series as in (2.7). Here h plays the role of the mean depth of the shallow water fluid, hence h is often referred to as the equivalent depth. If we rewrite (2.21) together with (2.8c) and (2.8e) we obtain

$$\frac{\partial \phi}{\partial p} + \frac{RT}{p} = 0, \tag{2.24a}$$

$$-i\sigma T + \left(\frac{\partial \bar{T}}{\partial p} - \frac{R\bar{T}}{pc_p}\right)\omega = \frac{Q}{c_p}, \tag{2.24b}$$

$$-i\sigma\phi - gh \frac{\partial \omega}{\partial p} = 0. \tag{2.24c}$$

Now we note that there are no p-derivatives in the system (2.23) and no y-derivatives in the system (2.24). Thus we have taken the system (2.8), in which all the equations are coupled in their y and p dependencies, and decoupled it to obtain the system (2.23), which completely determines the y-structure, and the system (2.24), which completely determines the p-structure. The sole remaining link between the two systems is the quantity gh. In some wave-CISK studies, such as Hayashi (1970) and Stark (1976), the validity of these two systems was anticipated and they were used in the analysis without justification. Here a rigorous justification for their use has been provided.

In order to obtain the dispersion relation for an equatorial beta-plane, we use the equation which governs the y-structure of v. Because of the decoupling described above, this equation may be derived from the system (2.23). Eliminating u from (2.23a) and (2.23b) gives

$$(\sigma^2-f^2)v + (i\sigma \frac{\partial}{\partial y} + ikf)\phi = 0. \tag{2.25}$$

Eliminating u from (2.23a) and (2.23c) gives

$$(i\sigma \frac{\partial}{\partial y} - ikf)v + (\frac{\sigma^2}{gh} - k^2)\phi = 0. \tag{2.26}$$

We now operate on (2.26) with $i\sigma\, \partial/\partial y + ikf$ and substitute from (2.25) to find

$$\frac{\partial^2 v}{\partial y^2} + (-\frac{k\beta}{\sigma} + \frac{1}{gh} (\sigma^2-f^2) - k^2)v = 0. \tag{2.27}$$

Following Lindzen (1967) we define

$$c_1 = \frac{\beta^2}{gh}, \tag{2.28}$$

$$c_2 = - \frac{k\beta}{\sigma} - k^2 + \frac{\sigma^2}{gh}, \tag{2.29}$$

$$\xi = c_1^{\frac{1}{4}} y. \tag{2.30}$$

Substituting (2.28) - (2.30) into (2.27) we obtain

$$\frac{\partial^2 v}{\partial \xi^2} + (c_2 c_1^{-\frac{1}{2}} - \xi^2)v = 0. \tag{2.31}$$

We choose the boundary conditions to be

$$v \to o \text{ as } \xi \to \pm \infty. \tag{2.32}$$

By assuming

$$v(\xi) = e^{-\xi^2/2} V(\xi), \tag{2.33}$$

which automatically satisfies (2.32), it may be shown that the solution to (2.31) is given by

$$v_n(\xi) = e^{-\xi^2/2} H_n(\xi), \tag{2.34}$$

where

$$c_2 c_1^{-\frac{1}{2}} - 1 = 2n, \tag{2.35}$$

and $H_n(\xi)$ is the Hermite polynomial of order n. Using (2.28) and (2.29), (2.35) may be rewritten as

$$\sigma^3 - (k^2 gh + \beta\sqrt{gh}(2n+1))\sigma - k\beta gh = 0, \tag{2.36}$$

which is the dispersion relation for an equatorial beta-plane.

We now derive the boundary conditions for the vertical structure equation (2.19). At the lower boundary we require

$$w = \frac{1}{g}\frac{d\phi}{dt} = 0. \tag{2.37}$$

Expanding the total derivative as in (2.2), linearizing, assuming solutions in the form of a Fourier series as in (2.7), and using (2.4) we find

$$-i\sigma\phi - \frac{R\bar{T}}{p}\,\omega = 0. \tag{2.38}$$

Now ϕ is eliminated by (2.24c) to yield

$$gh\,\frac{\partial\omega}{\partial p} - \frac{R\bar{T}}{p}\,\omega = 0, \tag{2.39}$$

or, after separating variables as in (2.16),

$$gh\,\frac{dW}{dp} - \frac{R\bar{T}}{p}\,W = 0. \tag{2.40}$$

At the upper boundary we apply the so-called rigid lid condition which requires $\omega = 0$ or, equivalently, $W = 0$. Thus, letting p_{00} denote the lower boundary and p_T the upper boundary, the complete vertical structure problem may be stated as

$$\frac{d^2W}{dp^2} + \frac{S}{gh}\,W = -\frac{\kappa J}{ghp}, \tag{2.41}$$

$$gh\,\frac{dW}{dp} - \frac{R\bar{T}}{p}\,W = 0 \text{ at } p = p_{00}, \tag{2.42}$$

$$W = 0 \text{ at } p = p_T. \tag{2.43}$$

The method for obtaining growth rates may now be made clear. It is shown in chapter 4 that when J is parameterized in terms of W, the vertical structure problem may be solved numerically as a generalized matrix eigenvalue problem where gh is the eigenvalue. For any eigenvalue, the dispersion relation (2.36) is solved yielding three roots for the quantity σ. Recalling that σ may be complex and using (2.7) it is easily shown that Re$\{\sigma\}$ determines the frequency of the wave and Im$\{\sigma\}$ determines the exponential growth rate.

3. CUMULUS PARAMETERIZATION

This chapter presents the details of the cumulus parameterization schemes used in the model. In section 3.1 a modified form of the parameterization originally developed by Stevens and Lindzen is presented. A simplified form of the parameterization of Arakawa and Schubert is given in section 3.2.

3.1 Stevens and Lindzen Parameterization

Stevens and Lindzen parameterization is based upon the fact that the net release of the latent heat of vaporization in a column must be balanced by the precipitation in that column. Thus we write

$$\int_{p_{CT}}^{p_B} Q \frac{dp}{g} = LP, \tag{3.1}$$

where p_{CT} and p_B are the upper and lower boundaries of the heated region, L is the latent heat of vaporization and P is the precipitation in units of $kgm^{-2}s^{-1}$.

We relate P to the large-scale vertical velocity as follows. The large-scale moisture budget may be written

$$\frac{\partial q}{\partial t} + \underset{\sim}{v}\cdot\nabla q + \omega \frac{\partial q}{\partial p} = E - C, \tag{3.2}$$

where E and C are evaporation and condensation in units of s^{-1}, q is the

mixing ratio, $\underset{\sim}{v}$ is the horizontal velocity vector and ∇ is the horizontal del operator at constant p. If we neglect the storage of water vapor given by $\partial q/\partial t$ and use the continuity equation (2.1d) we may write (3.2) as

$$\nabla \cdot q\underset{\sim}{v} + \frac{\partial}{\partial p}(q\omega) = E - C. \tag{3.3}$$

Upon integrating throughout the depth of the model atmosphere, and assuming either $\omega = 0$ or $q = 0$ at the upper boundary we find

$$P = -\int_{p_T}^{p_{00}} (E - C)\frac{dp}{g} = -\int_{p_T}^{p_{00}} \nabla \cdot q\underset{\sim}{v}\frac{dp}{g} - \frac{1}{g} q(p_{00})\,\omega(p_{00}), \tag{3.4}$$

Linearizing about a basic state defined by $\bar{P} = 0$, assuming $q = \bar{q}(p)$, using the continuity equation (2.6d) and either of the conditions at the upper boundary given above, we may show, after some manipulation, that

$$P' = -\frac{1}{g}\int_{p_T}^{p_{00}} \omega' \frac{d\bar{q}}{dp}\,dp. \tag{3.5}$$

Careful attention to the details of the above manipulation reveals that it is not necessary to assume $\omega'(p_{00}) = 0$ since $\omega'(p_{00})$ cancels out of the equation. We have now related the precipitation to the large-scale vertical velocity.

The profile of $\bar{q}$ may be specified in many ways. Stevens and Lindzen originally considered $\bar{q}$ given by

$$\bar{q} = \begin{cases} q_m \text{ (= constant)}, & p_m \le p \le p_{00} \\ 0, & p_T \le p \le p_m \end{cases} \tag{3.6}$$

where p_m is a specified pressure corresponding to the top of the moist layer. With this profile, (3.5) becomes, after careful evaluation of the integral,

$$P' = -\frac{1}{g} q_m \omega'(p_m). \tag{3.7}$$

Note that P' is related to the vertical velocity at only one level. Here we follow Davies (1980) and let $\bar{q}$ be given by

$$\bar{q} = \begin{cases} q_a \text{ (= constant)}, & p_a \le p \le p_{00} \\ q_a e^{-\delta(p_a - p)}, & p_d \le p \le p_a \\ 0, & p_T \le p < p_d \end{cases} \tag{3.8}$$

where δ and q_a are constants. As $\delta \to \infty$ this profile approaches the simple profile discussed above, thus a finite value for δ allows us to use a more realistic moisture profile. With $\bar{q}$ given by (3.8), (3.5) becomes, again after careful evaluation of the integral,

$$P' = -\frac{q_a \delta}{g} \int_{p_d}^{p_a} \omega' e^{-\delta(p_a - p)} dp - \frac{1}{g} \bar{q}(p_d)\, \omega'(p_d). \tag{3.9}$$

Here we note that P' is related to the vertical velocity at every level in the interval $p_d \le p \le p_a$.

We now relate the heating to the large-scale vertical velocity. Linearizing (3.1), substituting from (3.9), using (2.7), (2.16) and (2.17), we may show that

$$\int_{p_{CT}}^{p_B} J dp = -L q_a \delta \int_{p_d}^{p_a} W e^{-\delta(p_a - p)} dp - L\bar{q}(p_d)\, W(p_d). \tag{3.10}$$

The vertical profile of the heating is specified by writing

$$J(p) = \alpha e^{bp} \sin\pi \frac{p-p_B}{p_{CT}-p_B}. \tag{3.11}$$

The constant b determines the level of maximum heating. The constant α is the magnitude of the heating and is determined by substituting (3.11) into (3.10). With α determined in this manner (3.11) becomes

$$J(p) = -\frac{L}{a} e^{bp} \sin\pi \frac{p-p_B}{p_{CT}-p_B} \left[q_a \delta \int_{p_d}^{p_a} W(p) e^{-\delta(p_a-p)}\, dp \right.$$

$$\left. + \bar{q}\,(p_d) W(p_d)\right], \tag{3.12}$$

where

$$a = \int_{p_{CT}}^{p_B} e^{bp} \sin\pi \frac{p-p_B}{p_{CT}-p_B}\, dp. \tag{3.13}$$

We have now parameterized the heating J in terms of the large-scale vertical velocity W.

To summarize, we used a large-scale moisture budget to relate the precipitation to the large-scale vertical velocity. Then, we specified the vertical profile of the heating and, using the constraint that the net latent heat released in a column must balance the precipitation in that column, we determined the magnitude of the heating as a function of the large-scale vertical velocity.

3.2 Arakawa and Schubert Parameterization

The parameterization theory developed by Arakawa and Schubert describes the interaction between an ensemble of cumulus clouds and the large-scale environment. The reader is referred to Arakawa and Schubert

(1974) and Schubert (1974) for a complete discussion of the original theory. Further discussion may be found in Hack (1977) and Silva Dias and Schubert (1977).

In order to make the problem more tractable mathematically we make the following simplifications to the original theory:

(i) virtual temperature effects are neglected,

(ii) surface energy fluxes are neglected,

(iii) radiative effects are neglected,

(iv) the height of the sub-cloud mixed layer is constant,

(v) the thermal properties of the mixed layer are constant,

(vi) cloud base for all cloud types is at the top of the mixed layer.

Numerical considerations dictate an additional change from the original formulation of the theory. In Arakawa and Schubert (1974), the fractional rate of entrainment was the spectral parameter assumed to fully characterize each cloud type in the ensemble. In this formulation, the pressure where detrainment occurs (cloud top) for a given entrainment rate is a function of time. In a vertically discrete model it is difficult to allow for a cloud top which does not always coincide with one of the vertical levels, therefore, following Hack (1977), we let the spectral parameter be the detrainment level pressure instead of the fractional rate of entrainment. Now each cloud type in the ensemble is characterized by the pressure where it detrains. As a consequence of this reformulation, we must consider the fractional rate of entrainment to be a function of time since a change in the large-scale environment implies that any cloud type must entrain at a different rate in order to always detrain at the same level.

The equations in the theory have been conceptually grouped by Schubert (1974) into three categories: feedback, static control and dynamic control.

The feedback category describes the way in which a cumulus cloud ensemble produces time changes in the large-scale temperature and moisture fields. We define the convective scale fluxes of dry static energy s, moist static energy h and liquid water ℓ as

$$F_s(p) = \int_{p_T}^{p} \eta(p,\hat{p})[s_c(p,\hat{p}) - s(p)]m_B(\hat{p})d\hat{p}, \tag{3.14}$$

$$F_h(p) = \int_{p_T}^{p} \eta(p,\hat{p})[h_c(p,\hat{p}) - h(p)]m_B(\hat{p})d\hat{p}, \tag{3.15}$$

$$F_\ell(p) = \int_{p_T}^{p} \eta(p,\hat{p})\ell(p,\hat{p})m_B(\hat{p})d\hat{p}. \tag{3.16}$$

Here $s_c(p,\hat{p})$, $h_c(p,\hat{p})$ and $\ell(p,\hat{p})$ are the dry static energy, moist static energy and liquid water content at pressure p for the cloud type which detrains at pressure $\hat{p}$. All cloud variables shall have two arguments, the first being the pressure p and the second being the detrainment pressure $\hat{p}$ which is the spectral parameter characterizing each cloud type. The mass flux at level p due to cloud type $\hat{p}$ is $\eta(p,\hat{p})m_B(\hat{p})d\hat{p}$ where $m_B(\hat{p})d\hat{p}$ is the mass flux at cloud base and $\eta(p,\hat{p})$ is the normalized mass flux having the value 1 at cloud base. Using these definitions we may write the large-scale budgets of s and h as

$$\frac{\partial s}{\partial t} = - \underset{\sim}{v}\cdot\nabla s - \omega \frac{\partial s}{\partial p} + g \frac{\partial}{\partial p}(F_s - LF_\ell) + LR, \tag{3.17}$$

$$\frac{\partial h}{\partial t} = - \underset{\sim}{v}\cdot\nabla h - \omega \frac{\partial h}{\partial p} + g \frac{\partial}{\partial p} F_h. \tag{3.18}$$

The convective scale sink of liquid water (i.e., rain) R is defined by

$$R(p) = g \int_{p_T}^{p} \eta(p,\hat{p}) r(p,\hat{p}) m_B(\hat{p}) d\hat{p}, \tag{3.19}$$

where $g\eta(p,\hat{p})r(p,\hat{p})m_B(\hat{p})d\hat{p}$ is the rain at level p due to cloud type $\hat{p}$. Thus, if we know the properties of each cloud type and the cloud base mass flux m_B, we can determine the effect of the cloud ensemble on the time changes of the large-scale temperature and moisture fields.

In the static control category a simple cloud model is used to determine the properties of the cloud ensemble. The budgets for mass, moist static energy and total water substance for cloud type $\hat{p}$ are given by

$$\frac{\partial \eta(p,\hat{p})}{\partial p} = - \lambda(\hat{p})\eta(p,\hat{p}), \tag{3.20}$$

$$\frac{\partial}{\partial p} [\eta(p,\hat{p}) h_c(p,\hat{p})] = h(p) \frac{\partial \eta(p,\hat{p})}{\partial p}, \tag{3.21}$$

$$\frac{\partial}{\partial p}[\eta(p,\hat{p})(q_c(p,\hat{p})+\ell(p,\hat{p})] = q(p)\frac{\partial \eta(p,\hat{p})}{\partial p} + \eta(p,\hat{p})r(p,\hat{p}). \tag{3.22}$$

Here $q_c(p,\hat{p})$ is the cloud mixing ratio which may be determined from

$$q_c(p,\hat{p}) = q^*(p) + \frac{\gamma(p)}{1+\gamma(p)} \frac{1}{L} [h_c(p,\hat{p})-h^*(p)], \tag{3.23}$$

where

$$\gamma(p) = \frac{L}{c_p} \left(\frac{\partial q^*}{\partial T}\right)_p, \tag{3.24}$$

q^* is the saturation mixing ratio and h^* is the saturated moist static energy and $\lambda(\hat{p})$ is the fractional rate of entrainment for cloud type $\hat{p}$ which can be determined iteratively from (3.20) and (3.21) by requiring that

$$h_c(\hat{p},\hat{p}) = h^*(\hat{p}). \tag{3.25}$$

Since equations (3.20) - (3.22) are differential equations, they require boundary conditions which we choose to be

$$\begin{aligned} &\eta(p_B,\hat{p}) = 1, \quad h_c(p,\hat{p}) = h_M, \\ &q_c(p_B,\hat{p}) = q_M, \quad \ell(p_B,\hat{p}) = 0, \end{aligned} \tag{3.26}$$

where h_M and q_M are the moist static energy and mixing ratio in the mixed layer.

In the dynamic control category of the theory, the cloud base mass flux m_B is determined. We define the cloud work function, which is a measure of the bouyancy force associated with cloud type $\hat{p}$, as

$$A(\hat{p}) = \int_{\hat{p}}^{p_B} \frac{\eta(p,\hat{p})}{1+\gamma(p)} [h_c(p,\hat{p})-h^*(p)]\frac{dp}{p}. \tag{3.27}$$

Then we make the quasi-equilibrium assumption which states that $\partial A/\partial t = 0$. It may be shown that the time derivatives of η, h_c and h^* may be written in terms of the time derivatives of h and s. The prognostic equations for h and s, (3.17) and (3.18), involve terms of two types: the large-scale advective terms and the cloud terms which depend upon m_B. Thus the quasi-equilibrium assumption may be written, at least conceptually, as

$$\int_{p_T}^{p_B} K(\hat{p},\hat{p}')m_B(\hat{p}')d\hat{p}' + F(\hat{p}) = 0 \tag{3.28}$$

where the kernel $K(\hat{p},\hat{p}')$ depends upon h, s, η, h_c, s_c, ℓ and r and $F(\hat{p})$ represents the large-scale terms.

We now remark that the thermodynamic equation (3.17) is consistent with the thermodynamic equation (2.1e) only if we replace $\partial s/\partial t+\underset{\sim}{v}\cdot\nabla s$ with $c_p(\partial T/\partial t+\underset{\sim}{v}\cdot\nabla T)$. This is equivalent to saying $\omega = -\rho g w$. With this in mind, we identify Q in (2.1e) with the last two terms on the right hand side of (3.17).

The linearized form of the parameterization is now derived. We allow for a mean cloud structure given by $\bar{\lambda}$, $\bar{\eta}$, $\bar{h}_c$, $\bar{s}_c$, $\bar{q}_c$, $\bar{\ell}$ and $\bar{r}$ and we recall from Chapter 2 that the basic state given by (2.3) may not contain mean heating. Therefore, it may be shown from (3.14), (3.16), (3.17) and the remarks in the preceeding paragraph that $\bar{m}_B$ must be zero. With this fact the perturbation heating may be written as

$$\begin{aligned} Q' = g\frac{\partial}{\partial p}\int_{p_T}^{p} \bar{\eta}(p,\hat{p})[\bar{s}_c(p,\hat{p})-\bar{s}(p)-L\bar{\ell}(p,\hat{p})]m_B'(\hat{p})d\hat{p} \\ + gL\int_{p_T}^{p} \bar{\eta}(p,\hat{p})\bar{r}(p,\hat{p})m_B'(\hat{p})d\hat{p}, \end{aligned} \tag{3.29}$$

and the linearized form of (3.28) may be written as

$$\int_{p_T}^{p_B} \bar{K}(\hat{p},\hat{p}')m_B'(\hat{p}')d\hat{p}' + F(\hat{p}) = 0. \tag{3.30}$$

Here $F(\hat{p})$ involves the product of several mean quantities with ω'.

We now summarize. The mean quantities $\bar{\lambda}$, $\bar{\eta}$, $\bar{h}_c$, $\bar{s}_c$, $\bar{q}_c$, $\bar{\ell}$ and $\bar{r}$ may be determined by requiring that they satisfy the equations in the static control category. A parameterization of the rain $\bar{r}$ is also required. Once these quantities are known, the kernel $\bar{K}$ may be calculated and the Fredholm integral equation (3.30) may be solved to find m_B' in terms of ω'. Finally, using (3.29) we may determine Q' in terms of ω', or, after Fourier decomposition and separation of variables, J in terms of W. We shall find that J depends on W at every level in the interval $p_T \leq p \leq p_B$. Unfortunately, all of the above calculations must be done numerically. The following chapter presents some details of these numerical calculations.

4. DISCRETE FORMS AND SOLUTION TECHNIQUE

The vertical structure problem posed in Chapter 2 may be solved analytically only for simple profiles of basic state temperature and simple parameterizations of the heating. Such analytic solutions were obtained by Hayashi (1970), Lindzen (1974), Chang (1976) and others. In this research we use basic state temperature profiles and parameterizations which are sufficiently complex so that numerical techniques must be used to obtain solutions. For simplicity, we choose to use finite-difference methods. In section 4.1 the discrete form of the vertical structure equation and its boundary conditions is presented. Section 4.2 presents the discrete forms of the governing equations for the parameterizations. It is shown that once J is parameterized in terms of W, the vertical structure problem may be solved as a generalized matrix eigenvalue problem where $1/gh$ is the eigenvalue.

4.1 The Vertical Structure Problem

The vertical grid used in the model is shown in Fig. 4.1. The atmosphere is divided into K/2 layers, the lowest of which is the sub-cloud mixed layer. Excepting the mixed layer, the pressure depth of each layer is the same. The basic state quantities $\bar{T}$ and $\bar{q}$ are carried at every level. The vertical velocity W is carried at odd levels and the heating J is carried at even levels.

It is convenient to write the static stability S as $S = R\Gamma/p^2$ where $\Gamma = d\bar{T}/dz^* + \kappa\bar{T}$ is the static stability in $z^* = -\ell n(p/p_{00})$ coordinates.

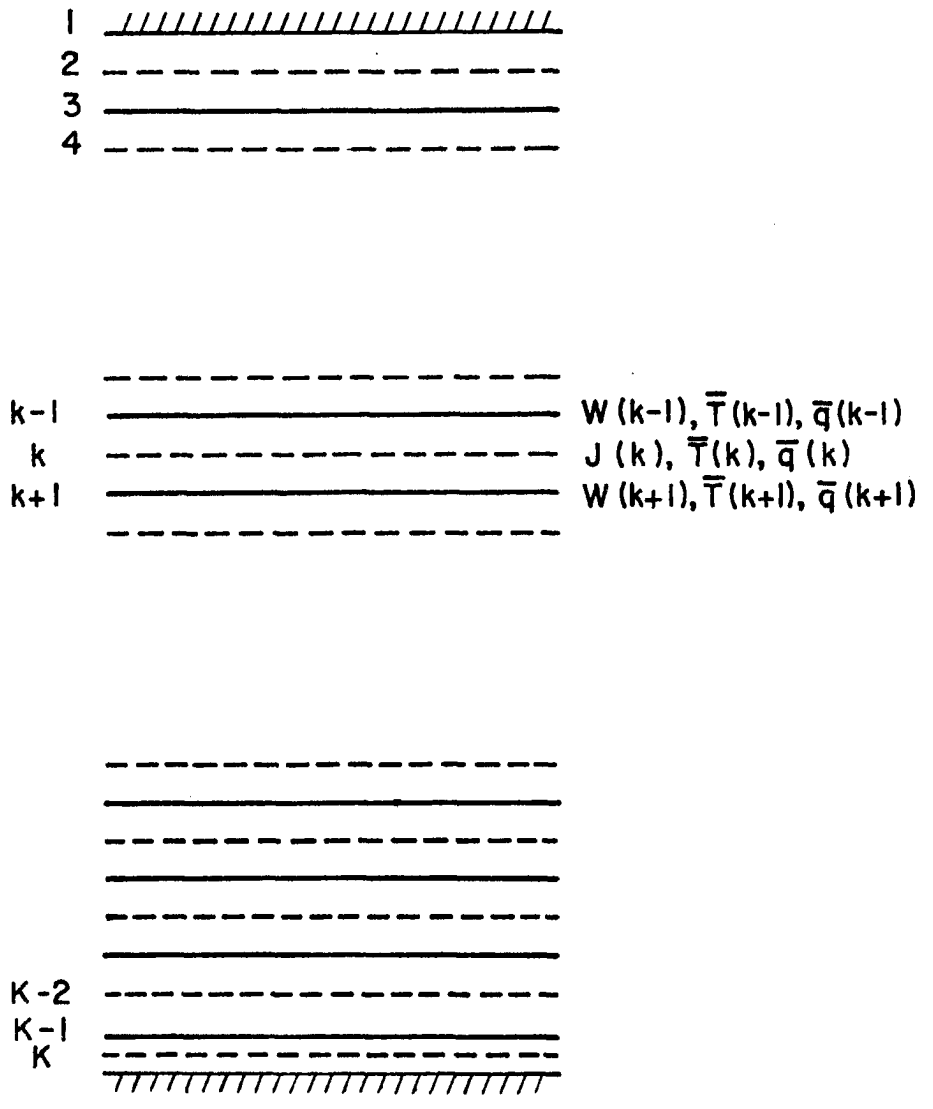

Fig. 4.1. Vertical grid used in the model.

The static stability Γ is often assumed to be constant; therefore, by writing S in this way we may compare the results obtained with a constant Γ with those obtained with a variable Γ.

For any interior odd level denoted by k, the finite-difference form of the vertical structure equation (2.41) is

$$\frac{W(k-2)-2\,W(k)+W(k+2)}{(\Delta p)^2} = \frac{-R\Gamma(k)}{ghp^2(k)}\,W(k) - \frac{\kappa}{2ghp(k)}\,(J(k-1)+J(k+1)). \tag{4.1}$$

Here $\Gamma(k)$ is determined from

$$\Gamma(k) = p(k)\,\left(\frac{R\bar{T}(k)}{c_p p(k)} - \frac{\bar{T}(k+1)-\bar{T}(k-1)}{\Delta p}\right) \tag{4.2}$$

and

$$\Delta p = p(k+1) - p(k-1). \tag{4.3}$$

The boundary conditions (2.42) and (2.43) are written in discrete form as

$$\frac{W(K+1)-W(K-1)}{p(K+1)-p(K-1)} = \frac{R\bar{T}(K+1)}{ghp(K+1)} \tag{4.4}$$

and

$$W(1) = 0. \tag{4.5}$$

Using these discrete forms we may write the complete vertical structure problem in matrix form as

$$A\,\underline{W} = 1/gh\,(B\,\underline{W} + C\,\underline{J}), \tag{4.6}$$

where A, B, and C are matrices of dimension $(K/2+1)\times(K/2+1)$, $\underline{W}$ is a vector of length K/2+1 containing the values of the vertical velocity at all odd levels, and $\underline{J}$ is a vector of length K/2+1 containing the values of the heating at all even levels. An additional even level above the model top has been defined solely in order to have K/2+1 levels at which J is carried.

It is shown in the next section that the cumulus parameterization schemes lead to a matrix equation of the form

$$\underline{J} = D\,\underline{W} \tag{4.7}$$

where D is a matrix of dimension (K/2+1)×(K/2+1). Using (4.7) and defining E = B + CD we may write (4.6) as

$$A\,\underline{W} = 1/gh\; E\,\underline{W} \tag{4.8}$$

which is a generalized matrix eigenvalue problem where 1/gh is the eigenvalue and W is the eigenvector. As mentioned in Chapter 2, growth rates corresponding to any eigenvalue are obtained by solving the dispersion relation (2.36) after substituting for gh. The vertical profile of the vertical velocity corresponding to any eigenvalue is contained in the eigenvector $\underline{W}$ while the vertical profile of the heating corresponding to any eigenvalue is contained in $\underline{J}$ and may be obtained from (4.7).

4.2 Cumulus Parameterization

In this section it is shown that the discrete forms of the cumulus parameterization schemes used in the model lead to a matrix equation of the form $\underline{J} = D\,\underline{W}$. The derivation of this equation is simple for Stevens and Lindzen parameterization and relatively complex for Arakawa and Schubert parameterization.

For Stevens and Lindzen parameterization a discrete form of (3.12) is used. We choose p_a and p_d to be at odd levels, p_{CT} to be at an even level, and p_B to be at level K-1. Using the trapezoidal rule to evaluate the integral in (3.12) we write the heating at any even level between p_B and p_{CT} as

$$J(k) = -\frac{L}{a} e^{bp(k)} \sin\pi \frac{p(k)-p(K-1)}{p(i_{CT})-p(K-1)}$$

$$\times \left[q_a \delta \sum_{i=i_d}^{i=i_a} \left(W(i-1)e^{-\delta(p(i_a)-p(i-1))} + W(i+1)e^{-\delta(p(i_a)-p(i+1))}\right)\right. \tag{4.9}$$

$$\left. \times \frac{\Delta p}{2} + \bar{q}(i_d)\, W(i_d)\right]$$

where i is odd, i_a and i_d are the odd levels where p_a and p_d are defined and i_{CT} is the even level where p_{CT} is defined. Using (4.9) the heating may easily be written in the form $\underline{J} = D\,\underline{W}$.

Before proceeding with Arakawa and Schubert parameterization we must calculate the quantities $\bar{s}$, $\bar{h}$, $\bar{h}^*$, $\bar{q}^*$ and γ. Calculation of the first three of these requires knowledge of the mean height $\bar{z}$. In the mixed layer, the temperature lapse rate is adiabatic and $\bar{z}$ may therefore be calculated from

$$\bar{z}(k) = \frac{c_p}{g}\left[\bar{T}_{00} - \bar{T}(k)\right]. \tag{4.10}$$

Above the mixed layer, $\bar{z}$ is calculated hydrostatically using

$$\bar{z}(k) = \bar{z}(k+1) + \frac{R}{2g}\left[\bar{T}(k) + \bar{T}(k+1)\right] \ell n \left(\frac{p(k+1)}{p(k)}\right). \tag{4.11}$$

Formulas for determining $\bar{q}^*$ and γ based on Teton's formula for the saturation mixing ratio e_s are given in Appendix B. Having obtained the quantities $\bar{z}$ and $\bar{q}^*$, we then calculate $\bar{s}$, $\bar{h}$ and $\bar{h}^*$ at any level k from

$$\left.\begin{aligned} \bar{s}(k) &= c_p \bar{T}(k) + g\bar{z}(k), \\ \bar{h}(k) &= \bar{s}(k) + L\bar{q}(k), \\ \bar{h}^*(k) &= \bar{s}(k) + L\bar{q}^*(k). \end{aligned}\right\} \tag{4.12}$$

As discussed in Chapter 3, we consider each cloud type to be characterized by the pressure where it detrains. In this model clouds are permitted to detrain at even levels from k = 2 to k = K-4. The cloud variables $\eta(p,\hat{p})$, $h_c(p,\hat{p})$, $q_c(p,\hat{p})$ and $\ell(p,\hat{p})$ are carried at odd levels and are denoted by $\eta(k-1,n)$, $h_c(k-1,n)$, $q_c(k-1,n)$ and $\ell(k-1,n)$.

The discrete forms of the equations in the static control category are now presented. The discrete mass budget for cloud type n is written

$$\eta(k-1,n) = \eta(k+1,n)\ (1+\lambda(n)\Delta p), \tag{4.13}$$

or, using the boundary condition $\eta(K-1,n) = 1$,

$$\eta(k-1,n) = (1+\lambda(n)\Delta p)^{(K-k)/2}. \tag{4.14}$$

The discrete moist static energy budget is written

$$\frac{\eta(k+1,n)h_c(k+1,n)-\eta(k-1,n)h_c(k-1,n)}{\Delta p} = h(k)\ \frac{\eta(k+1,n)-\eta(k-1,n)}{\Delta p}, \tag{4.15}$$

or, using (4.13),

$$h_c(k-1,n) = \frac{h_c(k+1,n)+\lambda(n)\Delta p h(k)}{1 + \lambda(n)\Delta p}\ . \tag{4.16}$$

We now introduce a crude parameterization of the rain $r(p,\hat{p})$ by writing $r(p,\hat{p}) = c_o(p,\hat{p})\ell(p,\hat{p})$ where $c_o(p,\hat{p})$ is an autoconversion coefficient. This parameterization essentially consists of converting a portion of the condensed liquid water into raindrops. Note that we have allowed the autoconversion coefficient to depend on pressure and cloud type. Using this parameterization the discrete budget for cloud water content

is written

$$\frac{\eta(k+1,n)(q_c(k+1,n)+\ell(k+1,n))-\eta(k-1,n)(q_c(k-1,n)+\ell(k-1,n))}{\Delta p}$$

$$= q(k)\,\frac{\eta(k+1,n)-\eta(k-1,n)}{\Delta p} + \eta(k+1,n)\; c_o(k,n)\ell(k-1,n), \qquad (4.17)$$

or, again using (4.13),

$$\ell(k-1,n) = \frac{(q_c+\ell)(k+1,n)-q_c(k-1,n)-\lambda(n)\Delta p[q_c(k-1,n)-q(k)]}{1+\lambda(n)\Delta p+c_o(k,n)\Delta p}\,. \qquad (4.18)$$

Here q_c is determined from

$$q_c(k-1,n) = q^*(k-1) + \frac{\gamma(k-1)}{1+\gamma(k-1)}\,\frac{1}{L}\,[h_c(k-1,n)-h^*(k-1)]. \qquad (4.19)$$

Although it is permitted to have cloud types which detrain as high as level 2, the actual detrainment level of the highest cloud type is determined by the $\bar{h}^*$ profile. An even level may not be a detrainment level for a cloud type if $\bar{h}^*$ at that level is greater than h_M since this would imply that the entrainment for such a cloud type would be negative.

Having determined from the above criterion how many actual cloud types exist, the following iterative scheme is used to calculate $\lambda(n)$ for each cloud type n. For any guess of $\lambda(n)$ we calculate $h_c(n+1,n)$ and $h_c(n-1,n)$ from (4.16) and $h_c(n,n)$ from

$$h_c(n,n) = \tfrac{1}{2}[h_c(n+1,n) + h_c(n-1,n)]. \qquad (4.20)$$

Next we calculate a function G(n) defined by

$$G(n) = \left|h^*(n) - h_c(n,n)\right|\,. \qquad (4.21)$$

If G(n) is less than some prescribed quantity ε, then we consider $\lambda(n)$ to be known to sufficient accuracy and we proceed to calculate $\lambda(n)$ for the next cloud type. If G(n) is greater than ε, then the secant method given by

$$\lambda^{\tau}(n) = \frac{\lambda^{\tau}(n)\, G^{\tau+1}(n) - \lambda^{\tau+1}(n)\, G^{\tau}(n)}{G^{\tau+1}(n) - G^{\tau}(n)} \tag{4.22}$$

where τ is the iteration index is used to calculate a new value of $\lambda(n)$. For this new value we calculate a new G(n) and test to see if it is less than ε. If it is not less than ε, we continue to make new guesses from (4.22) until G(n) is less than ε. The entire process is continued until $\lambda(n)$ for each cloud type is found. Note that the secant method defined by (4.22) requires two initial guesses. For the highest cloud type there is very little entrainment so it is best to choose two values near to zero. For the lower cloud types it is best to choose, whenever possible, the final iterative values of λ from the next two highest cloud types. Once $\lambda(n)$ is found for each n, h_c is known and η, ℓ, and q_c are calculated from (4.14), (4.18) and (4.19).

The equations comprising the feedback category are written in discrete form as

$$\begin{aligned}\frac{\partial s(k)}{\partial t} = \frac{\partial s(k)}{\partial t}\bigg|_{LS} + \frac{g}{\Delta p} \sum_{n'=n_{min}}^{K-4} \Big\{ &\eta(k+1,n')[s_c(k+1,n') - s(k+1) - \\ &- L\ell(k+1,n')] - \eta(k-1,n')[s_c(k-1,n') - s(k-1) - L\ell(k-1,n')] \Big\} M_B(n') \\ + Lg \sum_{n'=n_{min}}^{K-4} &\eta(k+1,n') c_o(k,n') \ell(k-1,n') M_B(n'),\end{aligned} \tag{4.23}$$

$$\frac{\partial h(k)}{\partial t} = \frac{\partial h(k)}{\partial t}\bigg|_{LS} + \frac{g}{\Delta p}\sum_{n'=n_{min}}^{K-4}\Big\{\eta(k+1,n')[h_c(k+1,n')-h(k+1)] - \eta(k-1,n')[h_c(k-1,n')-h(k-1)]\Big\}M_B(n') \tag{4.24}$$

where k is even, n' is even, n_{min} is the level where the highest cloud type detrains and

$$\frac{\partial s(k)}{\partial t}\bigg|_{LS} = - \underset{\sim}{v}(k)\cdot\nabla s(k) - \omega(k)\frac{\partial s(k)}{\partial p}, \tag{4.25}$$

$$\frac{\partial h(k)}{\partial t}\bigg|_{LS} = - \underset{\sim}{v}(k)\cdot\nabla h(k) - \omega(k)\frac{\partial h(k)}{\partial p}, \tag{4.26}$$

$$M_B(n') = \int_{\hat{p}(n')-\frac{\Delta p}{2}}^{\hat{p}(n')+\frac{\Delta p}{2}} m_B(\hat{p})d\hat{p} \ . \tag{4.27}$$

In the dynamic control category, the discrete version of the cloud work function is written

$$A(n) = \sum_{k'=n}^{K-2}\beta(k')\Big\{\eta(k'-1,n)[h_c(k'-1,n)-h^*(k')]\Delta p^-(k') + \eta(k'+1,n)[h_c(k'+1,n)-h^*(k')]\Delta p^+(k')\Big\} \tag{4.28}$$

where k' is even and

$$\beta(k') = \frac{1}{1+\gamma(k')}, \tag{4.29}$$

$$\Delta p^-(k') = \frac{2(p(k')-p(k'-1))}{p(k') + p(k'-1)}, \tag{4.30}$$

$$\Delta p^+(k') = \frac{2(p(k'+1)-p(k'))}{p(k'+1) + p(k')}. \tag{4.31}$$

A discrete form of the Fredholm integral equation (3.28) is derived in Appendix C and is written

$$\sum_{n'=n_{min}}^{K-4} K(n,n')M_B(n') + F(n) = 0 \tag{4.32}$$

where n' is even.

Recalling the discussion in Chapter 3, we write the linearized form of (4.32) as

$$\sum_{n'=n_{min}}^{K-4} \bar{K}(n,n')M_B'(n') + F(n) = 0. \tag{4.33}$$

The mean kernel $\bar{K}(n,n')$ depends on the mean quantities $\bar{\lambda}$, $\bar{\eta}$, $\bar{h}_c$, $\bar{s}_c$, $\bar{q}_c$ and $\bar{\ell}$. These mean quantities may be calculated by requiring that they satisfy the equations in the static control category. The large-scale forcing F(n) is a complicated expression involving the sum of several products of mean quantities with ω'. Keeping this in mind and performing the Fourier decomposition and separation of variables, we may write (4.33) in matrix form as

$$K \underline{M}_B + F \underline{W} = 0. \tag{4.34}$$

Here K is a matrix of dimension NxN where N is the number of cloud types, F is a matrix of dimension Nx(K/2+1), and $\underline{M}_B$ is a vector of length N containing the cloud base mass fluxes for each cloud type.

Using (4.23) and again performing the Fourier decomposition and separation of variables, the heating defined by (3.29) may be written in matrix form as

$$\underline{J} = H \underline{M}_B \tag{4.35}$$

where H is a matrix of dimension (K/2+1)xN. Solving (4.34) for $\underline{M}_B$ and using (4.35) we find that $\underline{J}$ may be written in the form $\underline{J} = D\ \underline{W}$.

We have now shown that the discrete versions of both parameterizations may be written in the form $\underline{J} = D\ \underline{W}$.

5. RESULTS

It was shown in Chapter 4 that when the heating is parameterized in terms of the vertical velocity, the vertical structure problem may be solved as a generalized matrix eigenvalue problem. The eigenvalues, along with the dispersion relation, determine the growth rates and phase speeds and the eigenvectors determine the vertical structure. In this chapter we present and discuss some results obtained by solving the vertical structure problem. Our primary objective is to compare the results obtained with Stevens and Lindzen parameterization (hereafter referred to as SL) with those obtained with Arakawa and Schubert parameterization (hereafter referred to as AS).

The atmosphere has been divided vertically into 11 layers. We have chosen the surface pressure to be 1011 mb, the sub-cloud mixed layer to extend from the surface to 965 mb, and the model top to be at 115 mb.

The profiles of basic state temperature $\bar{T}$ and basic state mixing ratio $\bar{q}$ are shown in Fig. 5.1. By definition, the sub-cloud mixed layer is characterized by a dry adiabatic temperature lapse rate and a constant mixing ratio. Above the mixed layer the mixing ratio has a roughly exponential decrease.

The static stability Γ, calculated from the $\bar{T}$ profile of Fig. 5.1, is shown in Fig. 5.2. In some studies, such as Chang (1976) and Stevens, et al. (1977), a constant value for Γ was assumed. In Table 5.1, the eigenvalues of the homogeneous vertical structure problem are

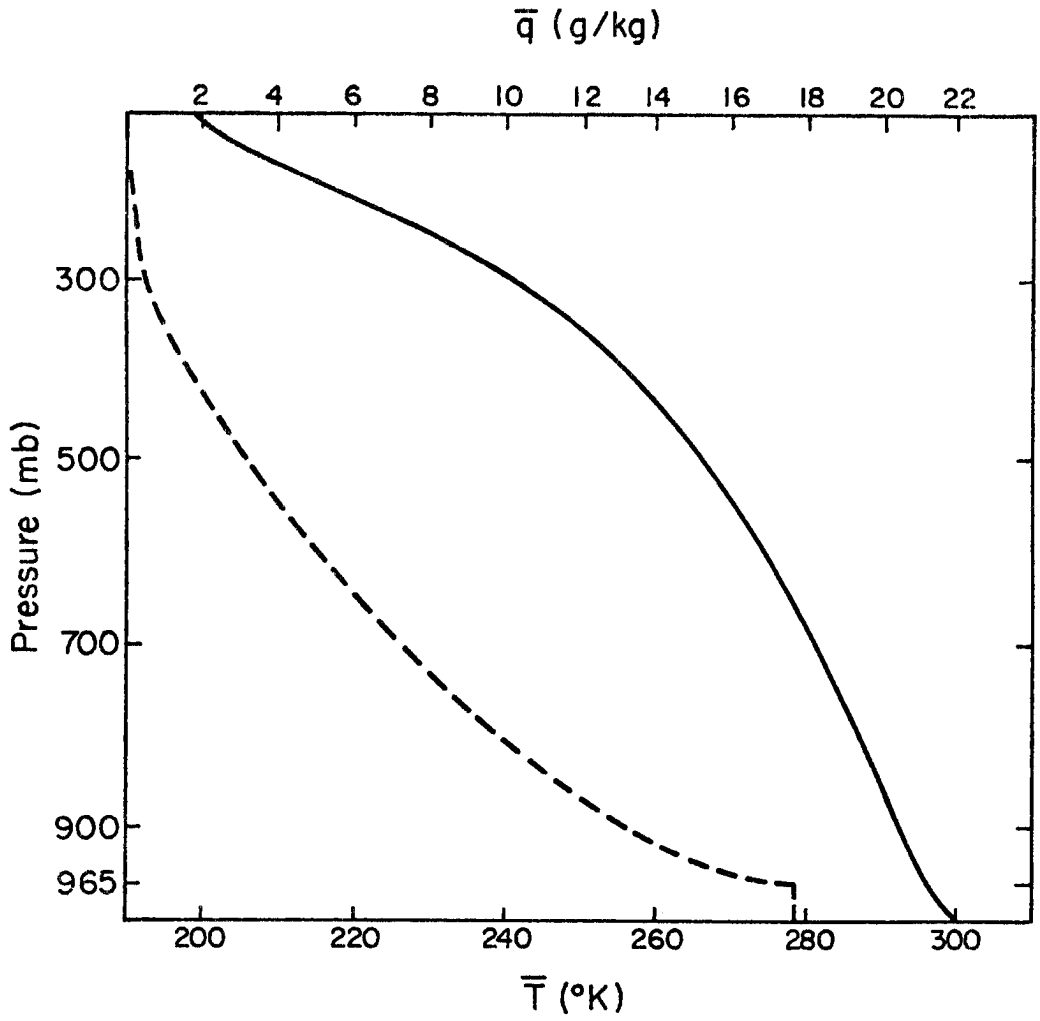

Fig. 5.1. Profiles of basic state temperature $\bar{T}$ (solid line) and basic state mixing ratio $\bar{q}$ (dashed line).

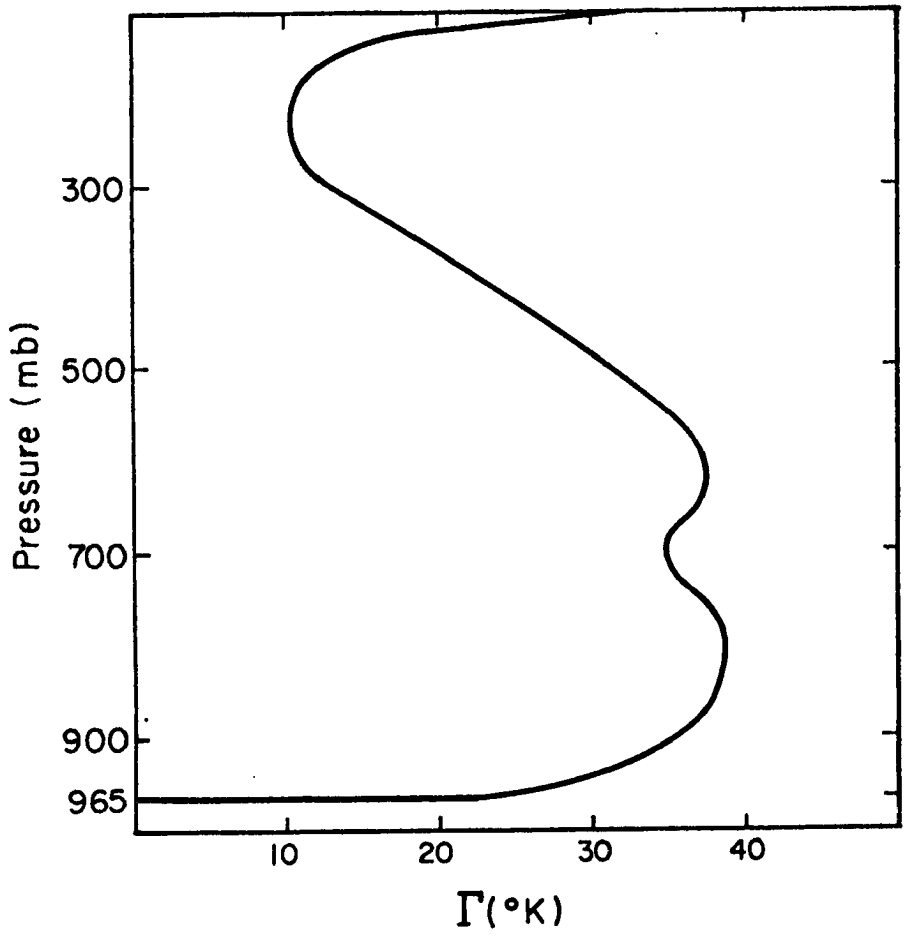

Fig. 5.2. The static stability Γ calculated from the basic state temperature profile of Fig. 5.1.

Vertical Mode	Constant Static Stability Γ=23.79°K	Static Stability of Fig. 5.2
0	282.6	284.3
1	53.54	50.03
2	28.68	25.36
3	19.61	17.91
4	14.69	13.74
5	11.46	11.10
6	9.16	9.50
7	7.43	8.61
8	6.06	7.42
9	4.91	6.06
10	3.56	3.41

Table 5.1 Phase speeds $\sqrt{gh}$ obtained from the homogeneous vertical structure problem for Γ=23.79°K=constant and for Γ given by Fig. 5.2. Units are m/s.

listed for the case when Γ is constant and for the case when Γ is given by the profile in Fig. 5.2. The eigenvalues are written in terms of $\sqrt{gh}$, which is the phase speed of a pure gravity wave. Mode zero is often referred to as the external mode while mode n is often referred to as the nth internal mode. We see that the primary effect of a variable static stability is to decrease the phase speeds of the lower order modes and increase the phase speeds of the higher order modes. The eigenvectors, or vertical structure functions, of the external and first three internal modes for both Γ profiles are shown in Fig. 5.3. Here we see that the levels where the internal modes attain a maximum or minimum are lower for a variable Γ. Later we shall see that varying the Γ profile as above produces a very noticable effect on the instabilities. Unless otherwise noted, all results presented from this point on are for the Γ profile given by Fig. 5.2.

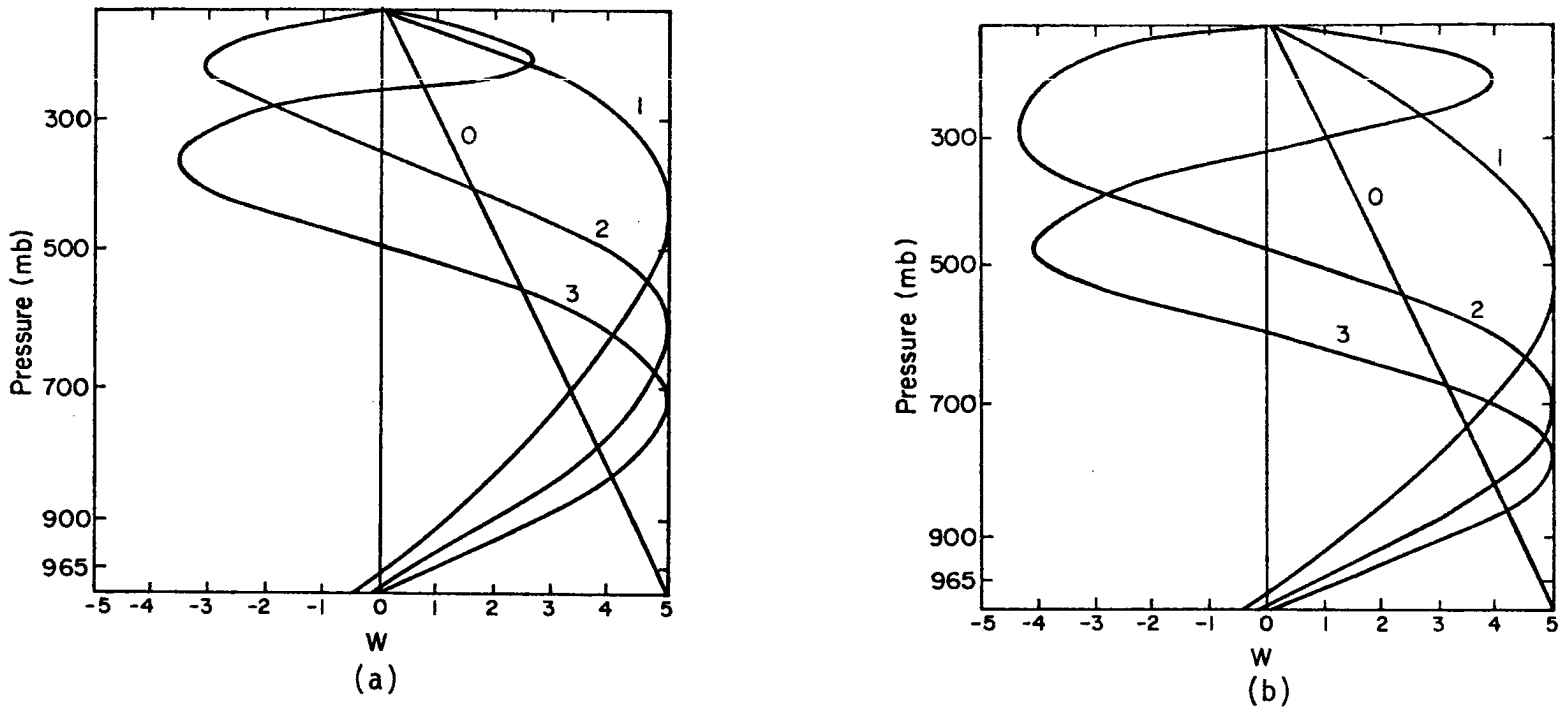

Fig. 5.3. Eigenvectors W for n = 0, 1, 2, 3, as labeled for (a) constant static stability $\Gamma = 23.79°K$ and (b) the static stability of Fig. 5.2.

We now present and discuss some results obtained using SL parameterization. The parameters p_{CT} and p_B are chosen to be 157.5 mb and 965 mb, respectively. We take the level of maximum heating, which determines the parameter b in (3.12), to be 455 mb. Chang (1976) studied the sensitivity to this parameter. Recall that we have chosen the $\bar{q}$ profile to be given by (3.8). In Fig. 5.4 several different profiles of $\bar{q}$ corresponding to different values of δ are shown. By comparison with Fig. 5.1, it may be seen that curve (a) is a reasonable approximation to the observed $\bar{q}$ profile.

In Fig. 5.5 we have plotted the set of eigenvalues gh as a function of q_a for the case where the moisture is constant from the surface to some pressure and zero thereafter, i.e., the profile originally considered by Stevens and Lindzen (1978). Since several figures of this nature will be presented, some preliminary explanation may be helpful. From the dispersion relation (2.36) we see that complex gh leads to complex σ and hence instability. Also, it may be demonstrated numerically that the instability generally increases as Im{gh} increases. In these figures we tend to see the coalescence of two modes with real equivalent depths into a single mode with complex equivalent depth. This coalescence coincides with the onset of the instability. Although the unstable modes come in complex conjugate pairs, we have plotted only the eigenvalue with positive imaginary part. Focusing on Fig. 5.5, it may be seen that instability first occurs for $q_a \cong 8.5$g/kg. However, when q_a increases to 10.5g/kg, the first and second internal modes coalesce to form an unstable mode. This unstable mode, although the second mode to become unstable as q_a increases, eventually attains a

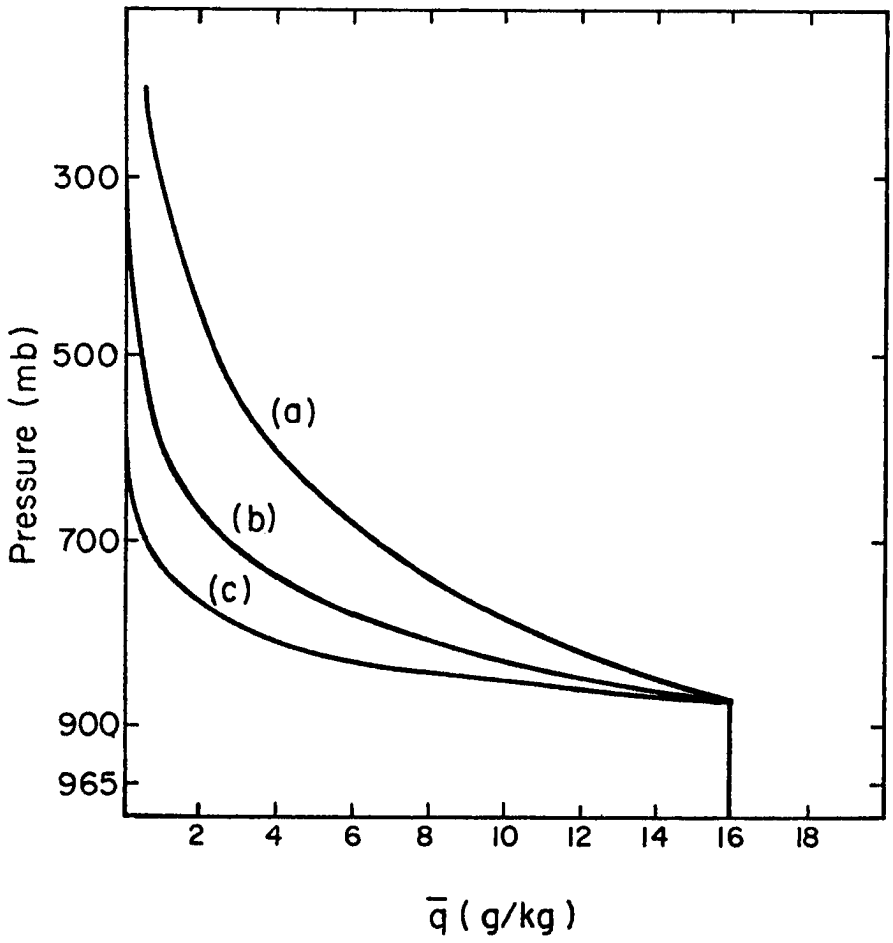

Fig. 5.4. Mixing ratio $\bar{q}$ calculated from (3.8) for p_a = 880 mb, p_d = 200 mb, q_a = 16 g/kg and (a) $\delta = 0.5\times10^{-2}\text{mb}^{-1}$, (b) $\delta = 1.0\times10^{-2}\text{mb}^{-1}$, (c) $\delta = 2.0\times10^{-2}\text{mb}^{-1}$.

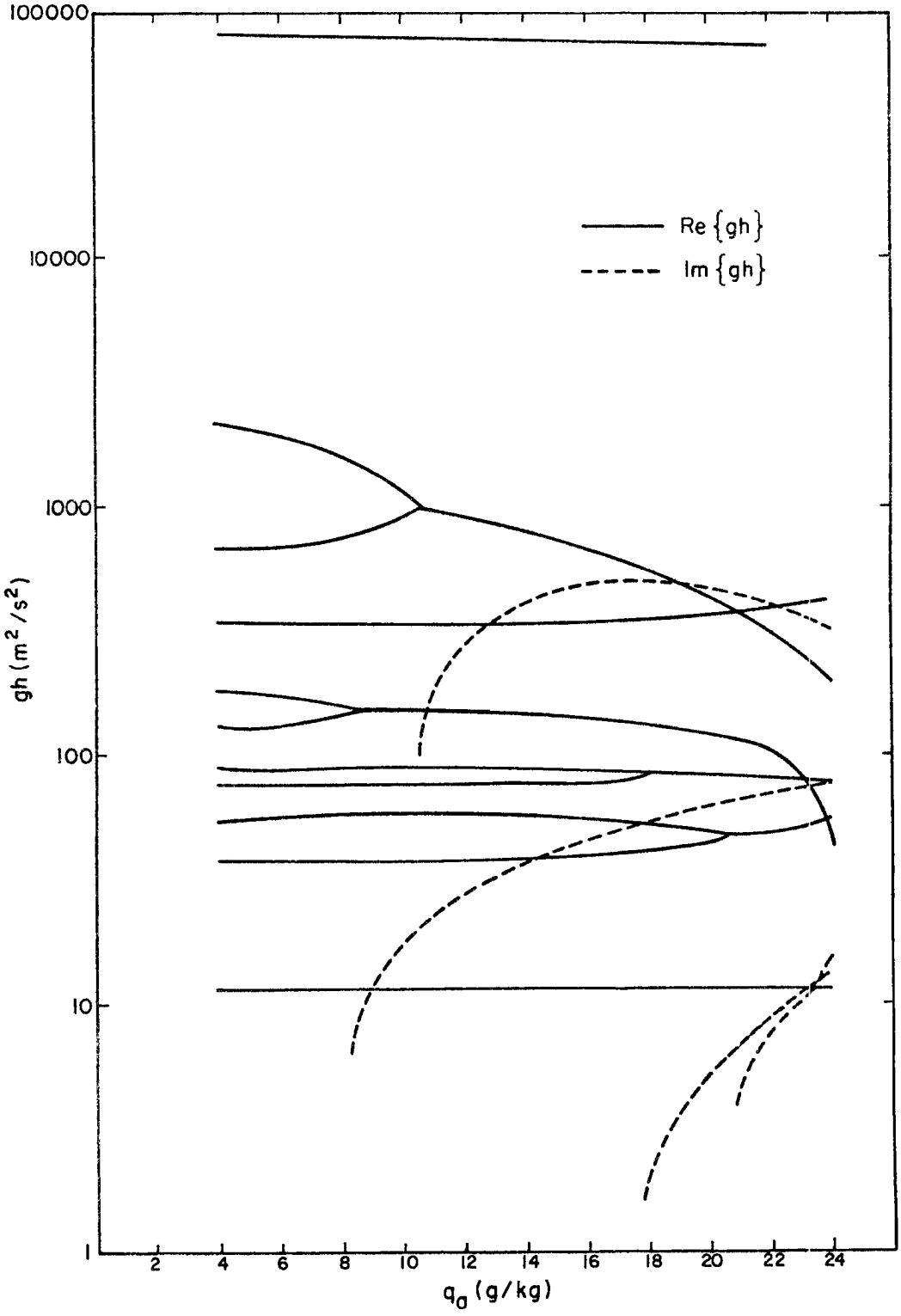

Fig. 5.5. Eigenvalues gh as a function of q_a for $p_a=p_d=795$ mb and $\delta = \infty$.

greater value of Im{gh} and hence a greater instability than the first unstable mode. As q_a increases even further two more unstable modes develop.

The e-folding time and phase speeds for the most unstable modes in Fig. 5.5 are shown in Fig. 5.6. Some preliminary explanation is also helpful here. For any given values of gh, horizontal wavelength and meridional mode n, the dispersion relation gives e-folding times and phase speeds for three wave types: eastward and westward moving gravity waves and westward moving Rossby waves. Since one possible application of the results of this research is in the study of squall lines and since squall lines may be associated with gravity waves, we choose to calculate e-folding times and phase speeds for a gravity wave of wavelength 300 km and meridional mode n = 1. Returning to Fig. 5.6, we confirm that the second mode to become unstable as q_a increases does attain a smaller e-folding time, or greater growth rate than the first mode which becomes unstable. The most unstable mode has the greater phase speed. The phase speeds are relatively unaffected by changes in q_a; however, as q_a increases through certain values the e-folding times may markedly increase.

The linearized thermodynamic equation consists of three terms: the local rate of change of temperature, the adiabatic cooling which may be written, after Fourier decomposition and separation of variables, as $-\Gamma W/p$, and the cumulus heating which may similarly be written J/c_p. In Fig. 5.7, we show, for the most unstable mode in Fig. 5.6 at q_a = 12.0 g/kg, the amplitude and phase of the vertical velocity, the cumulus heating, and the adiabatic cooling. Here we have assumed q_a = 12.0 g/kg = constant provides a reasonable approximation to the lower tropospheric

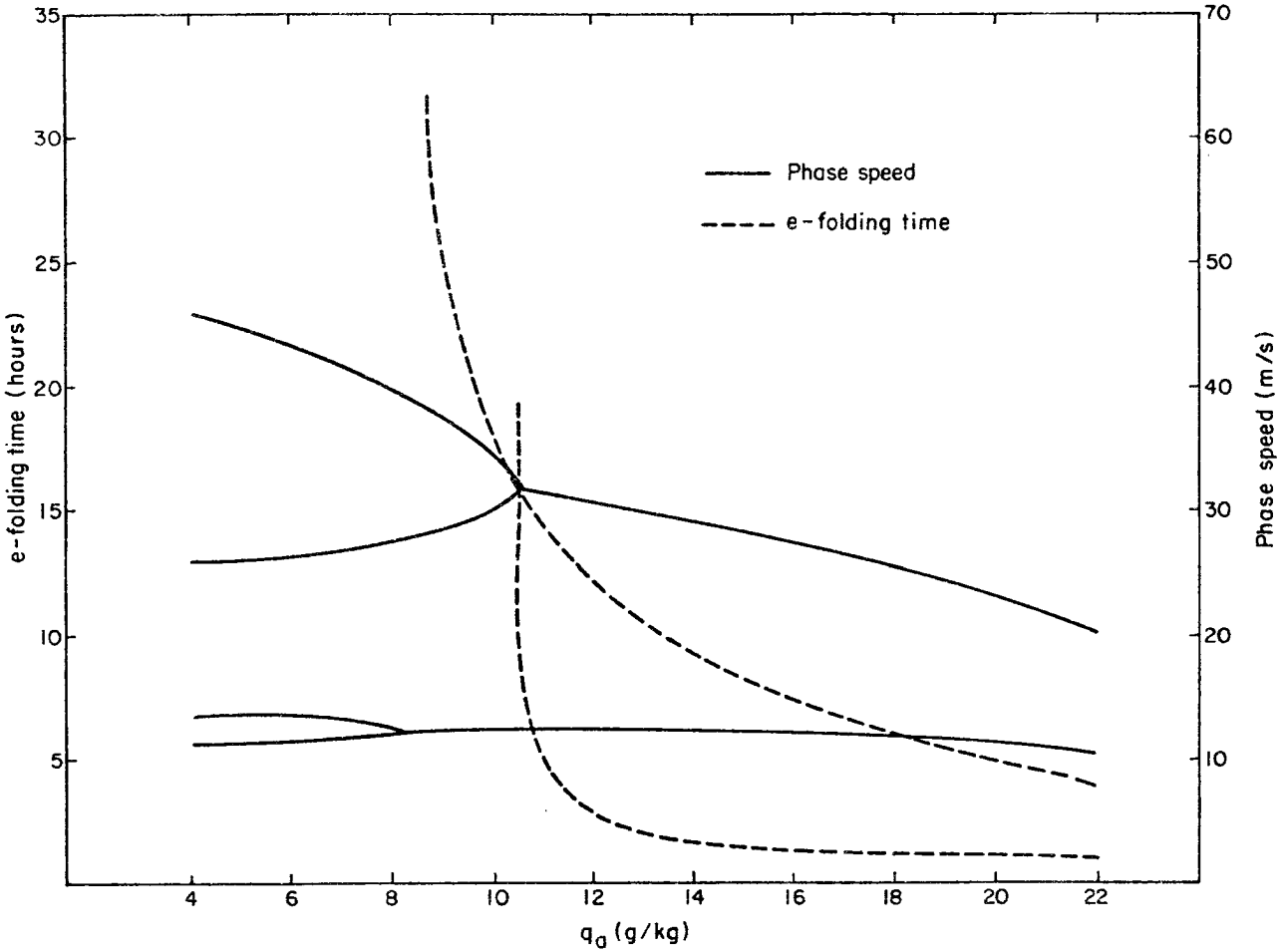

Fig. 5.6. The e-folding times and phase speeds as a function of q_a for the two most unstable modes of Fig. 5.5 computed for a gravity wave of wavelength 300 km and meridional mode n = 1.

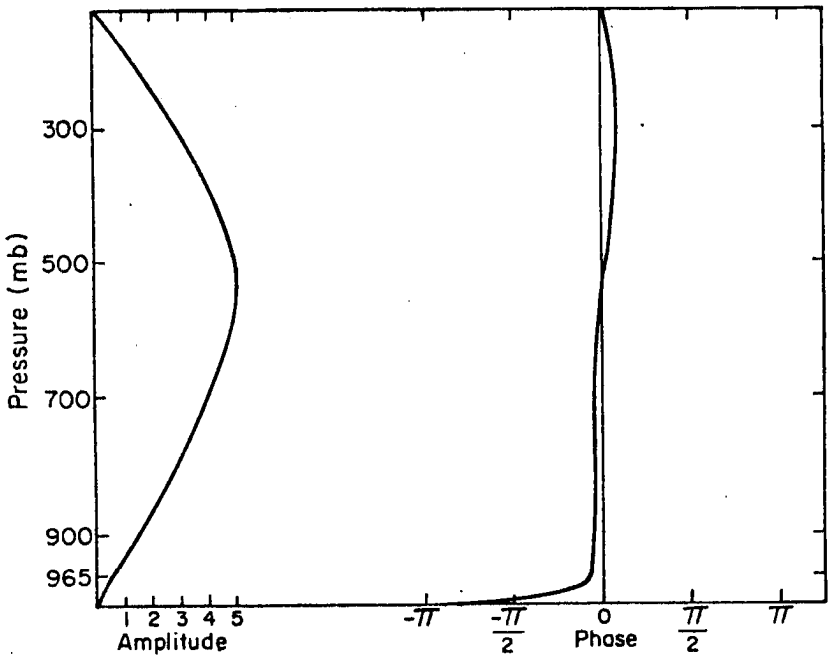

(a)

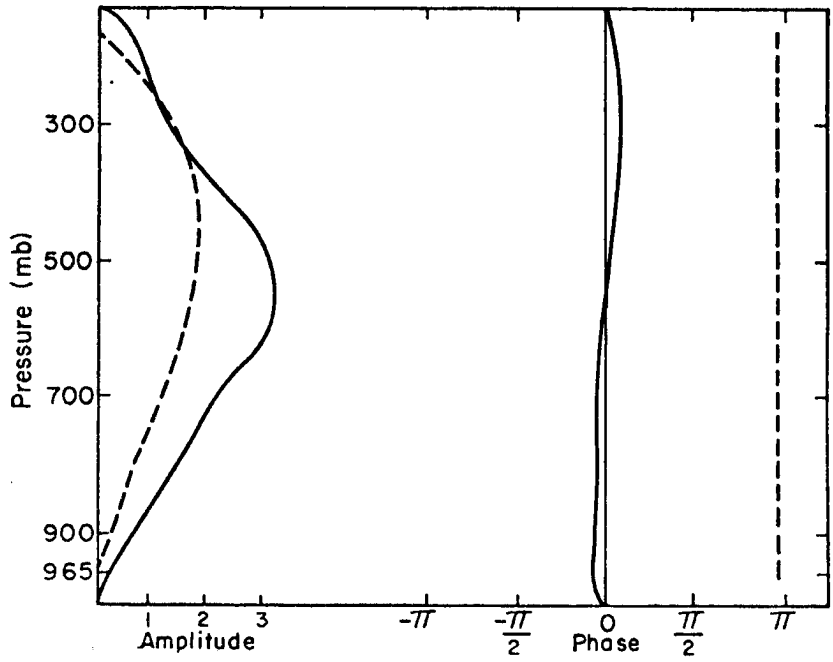

(b)

Fig. 5.7. Amplitude and phase of (a) the vertical velocity and (b) the adiabatic cooling (solid line) and cumulus heating (dashed line) for the most unstable mode in Fig. 5.6 at q_a = 12 g/kg.

moisture content. Recalling that W is negative for upward motion we see that the cumulus heating is in phase with the upward motion and does not tilt with height since it is related to the vertical velocity at only one level. The adiabatic cooling is greater than the cumulus heating at almost every level. The vertical velocity has a maximum near the middle troposphere and has very little tilt with height. Remember that the vertical profile of cumulus heating for SL parameterization is specified.

We now note that the eigenvalues discussed above are noticeably different for a constant Γ. For example, when q_a = 12.0 g/kg, the eigenvalue of the most unstable mode with a constant Γ equal to 23.79K is gh =171+59i m^2/s^2 while the eigenvalue of the most unstable mode with variable Γ is gh = 905+287i m^2/s^2. Thus, at least in this case, the instability is considerably reduced when a constant Γ is used.

So far we have presented results only for a very simple moisture profile. Fig. 5.8 shows the set of eigenvalues as a function of δ. Note that as δ increases there is very little change in either the real or imaginary parts of gh which implies that middle and upper tropospheric moisture plays a small role in SL parameterization.

Results obtained using AS parameterization are now presented and discussed. Whenever possible, a comparison will be made with the results obtained using SL parameterization. Vertical profiles of $\bar{h}$, $\bar{h}^*$ and $\bar{h}_c$ are shown in Fig. 5.9. The $\bar{h}^*$ profile, the value of $\bar{h}$ in the mixed layer and the number of layers in the model allow for nine cloud types. This is an improvement from Stark (1976) who had only four cloud types. The profile of the normalized mass flux $\bar{\eta}$ for each cloud type is shown in Fig. 5.10. Table 5.2 lists the value of the fractional entrainment rate $\bar{\lambda}$ for each cloud type.

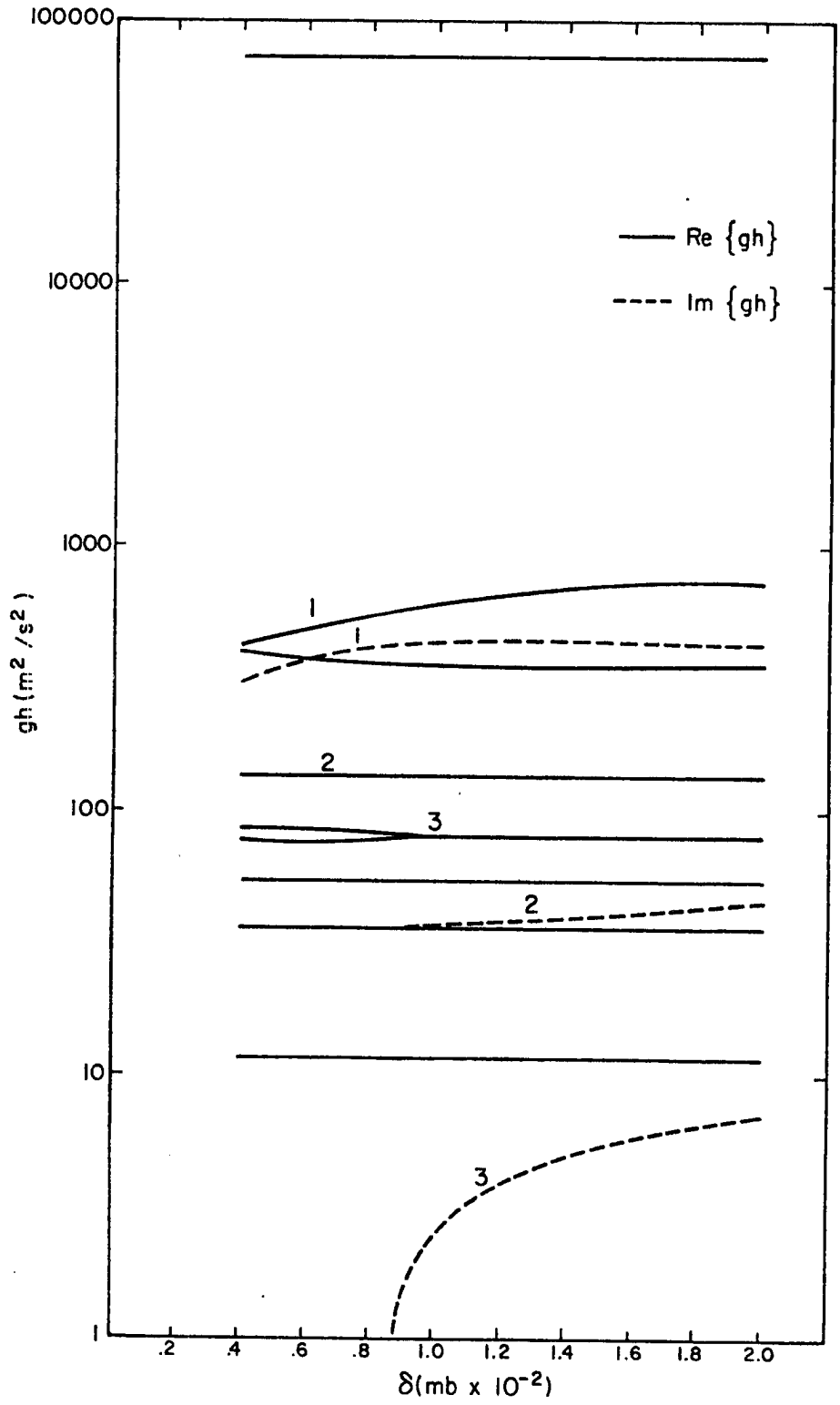

Fig. 5.8. Eigenvalues gh as a function of δ for p_a = 880 mb, p_d = 200 mb and q_a = 16 g/kg.

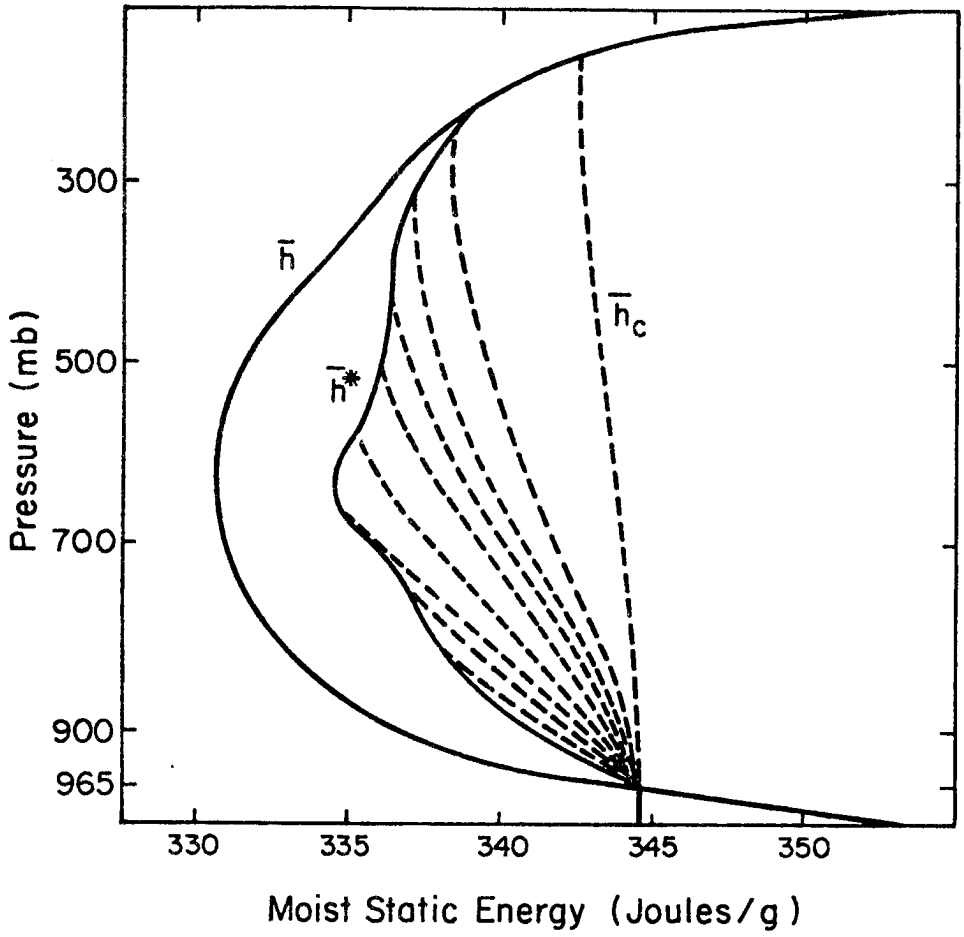

Fig. 5.9. Vertical profiles of $\bar{h}$, $\bar{h}^*$ and $\bar{h}_c$. Lines of $\bar{h}_c$ are dashed and each line corresponds to one of the nine cloud types present in the model.

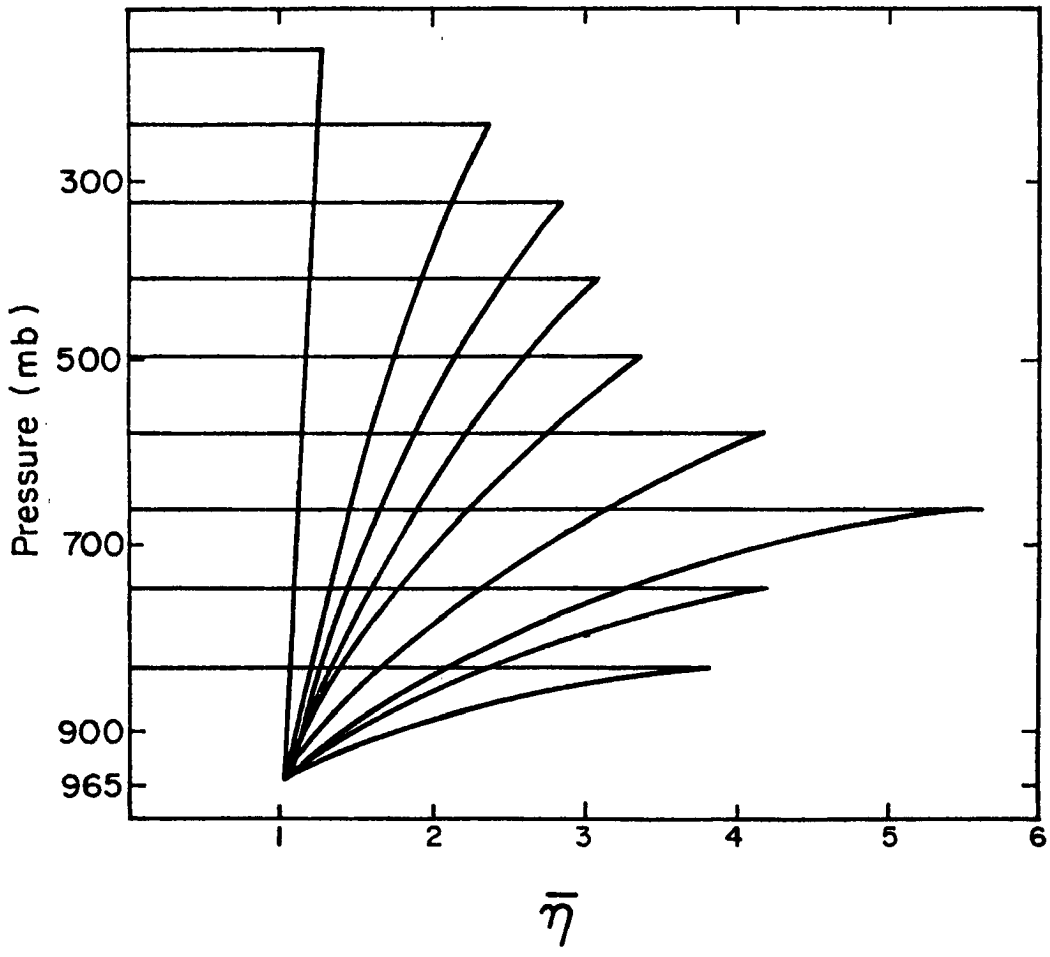

Fig. 5.10. Vertical profile of the normalized mass flux $\bar{\eta}$ for each cloud type.

$\hat{p}$(mb)	$\bar{\lambda}$(mb^{-1})
157.5	.00028626
242.5	.00123231
327.5	.00175591
412.5	.00221036
497.5	.00289031
582.5	.00441187
667.5	.00731829
752.5	.00873087
837.5	.01517879

Table 5.2 Fractional entrainment rate $\bar{\lambda}$ and detrainment pressure $\hat{p}$ for each cloud type.

The choice of a profile for the autoconversion coefficient c_o is difficult. A constant value, independent of cloud type, was proposed by Arakawa and Schubert (1974). Silva Dias and Schubert (1977) showed that this profile tends to underestimate the precipitation efficiency of deep clouds while overestimating it for shallow clouds. Consequently, they considered a profile where c_o varied with cloud type with the deeper clouds having greater values of c_o and hence greater precipitation efficiencies. In this research we consider the case where c_o is constant and the case when c_o is variable. For the variable case we let c_o be given by

$$c_o = \frac{b}{\pi} \cot^{-1} \left(\frac{\hat{p}-c}{a}\right) \tag{5.1}$$

where a, b and c are constants. Fig. 5.11 shows several profiles of c_o, each of which corresponds to a different value of b for fixed values of a and c. As b increases, the precipitation efficiency for all cloud

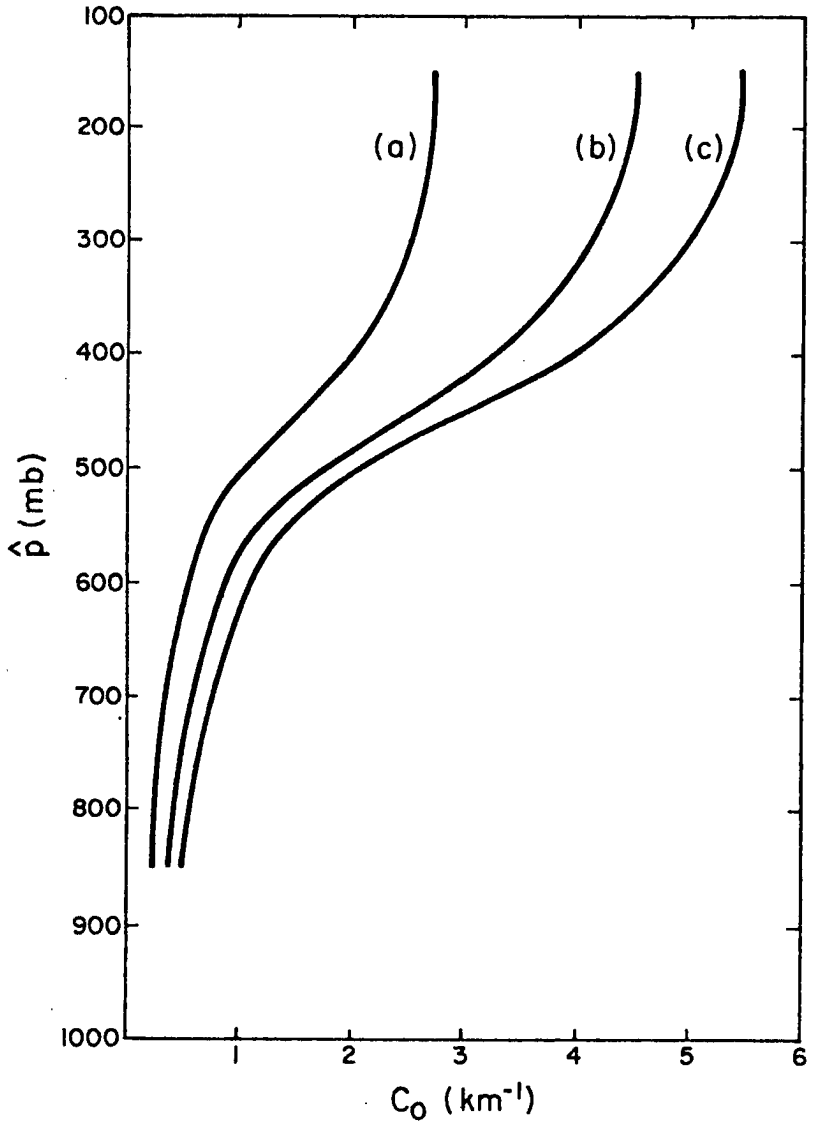

Fig. 5.11. Autoconversion coefficient c_o calculated from (5.1) for a = 90 mb, c = 450 mb and (a) b = 3 km^{-1}, (b) b = 5 km^{-1} and (c) b = 6 km^{-1}.

types increases; however, the increase is greater for higher cloud types than lower cloud types. The profile for $b = 5\ km^{-1}$ agrees well with the profile shown in Silva Dias and Schubert (1977). The quantity c_0 used in the discrete cloud total water budget is a function of pressure and has units of Pa^{-1}. It may be obtained from the c_0 values discussed above by multiplying those values by $R\bar{T}/pg$.

The set of eigenvalues as a function of c_0, where c_0 is constant and independent of cloud type, is shown in Fig. 5.12. The eigenvalues as a function of b are shown in Fig. 5.13. The two figures are qualitatively the same. Unstable modes first develop for $c_0 \cong 0.5\ km^{-1}$ and $b \cong 0.8\ km^{-1}$. As c_0 and b increase, additional unstable modes develop and, as in SL parameterization, these modes eventually attain greater values of Im{gh} and hence greater instabilities than the first modes which became unstable. Contrary to the results obtained with SL parameterization and the results obtained by Stark (1976), the first internal mode never coalesces to form an unstable mode. A possible explanation for this behavior is based on the fact that for SL parameterization, the vertical structure of the heating is specified and looks similar to the vertical structure of the first internal mode. Thus we might expect the unstable response to this specified heating to manifest itself primarily in the first internal mode. In AS parameterization, the vertical structure of the heating is not specified beforehand but is instead determined internally to the model. Therefore, there is no specified heating profile which might tend to force a response in some particular mode. Comparing with Fig. 5.5 we see that Re{gh} and Im{gh} for the unstable modes are smaller for AS parameterization than they are for SL parameterization.

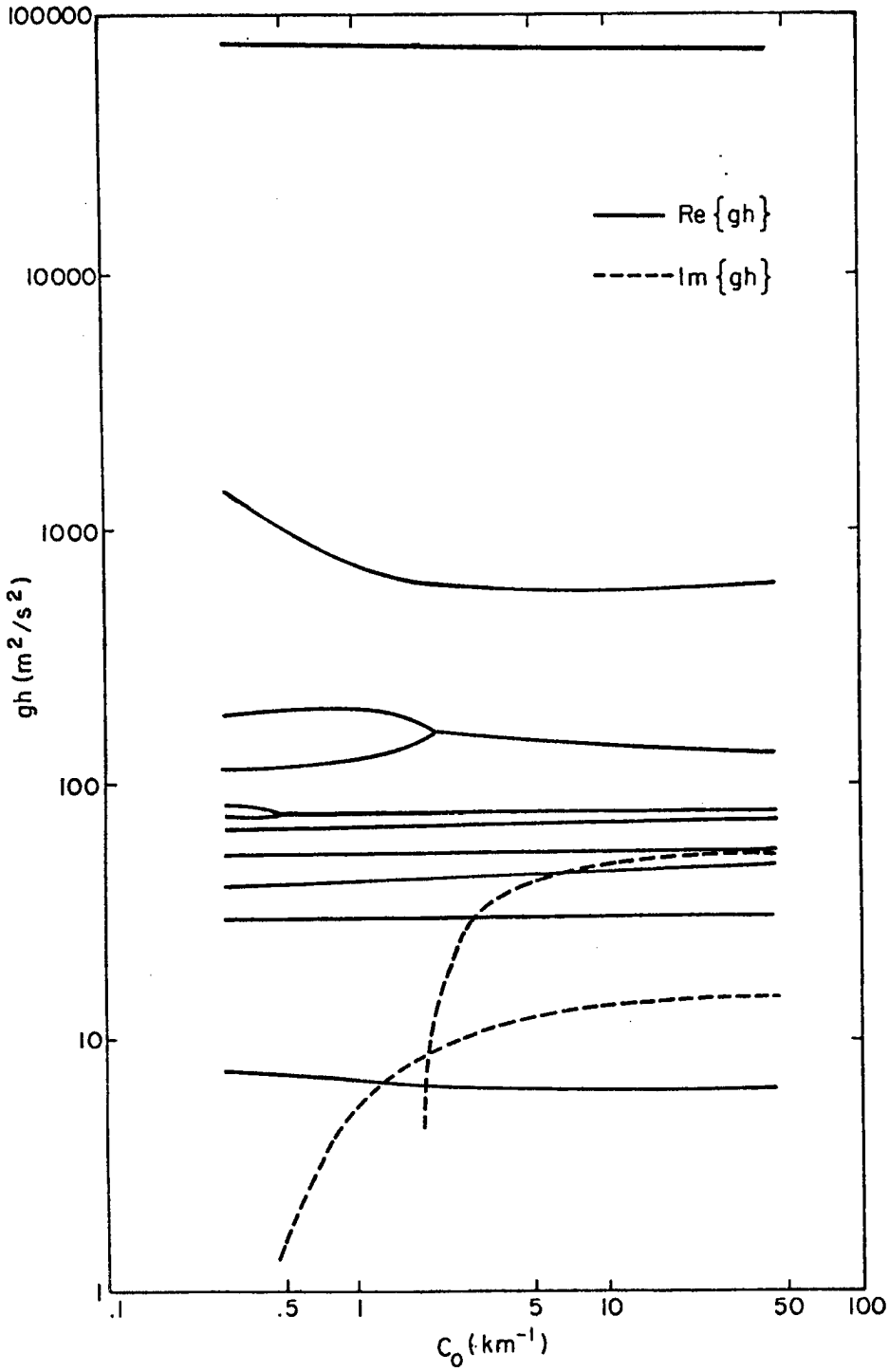

Fig. 5.12. Eigenvalues gh as a function of c_0 for the case where c_0 is constant and independent of cloud type.

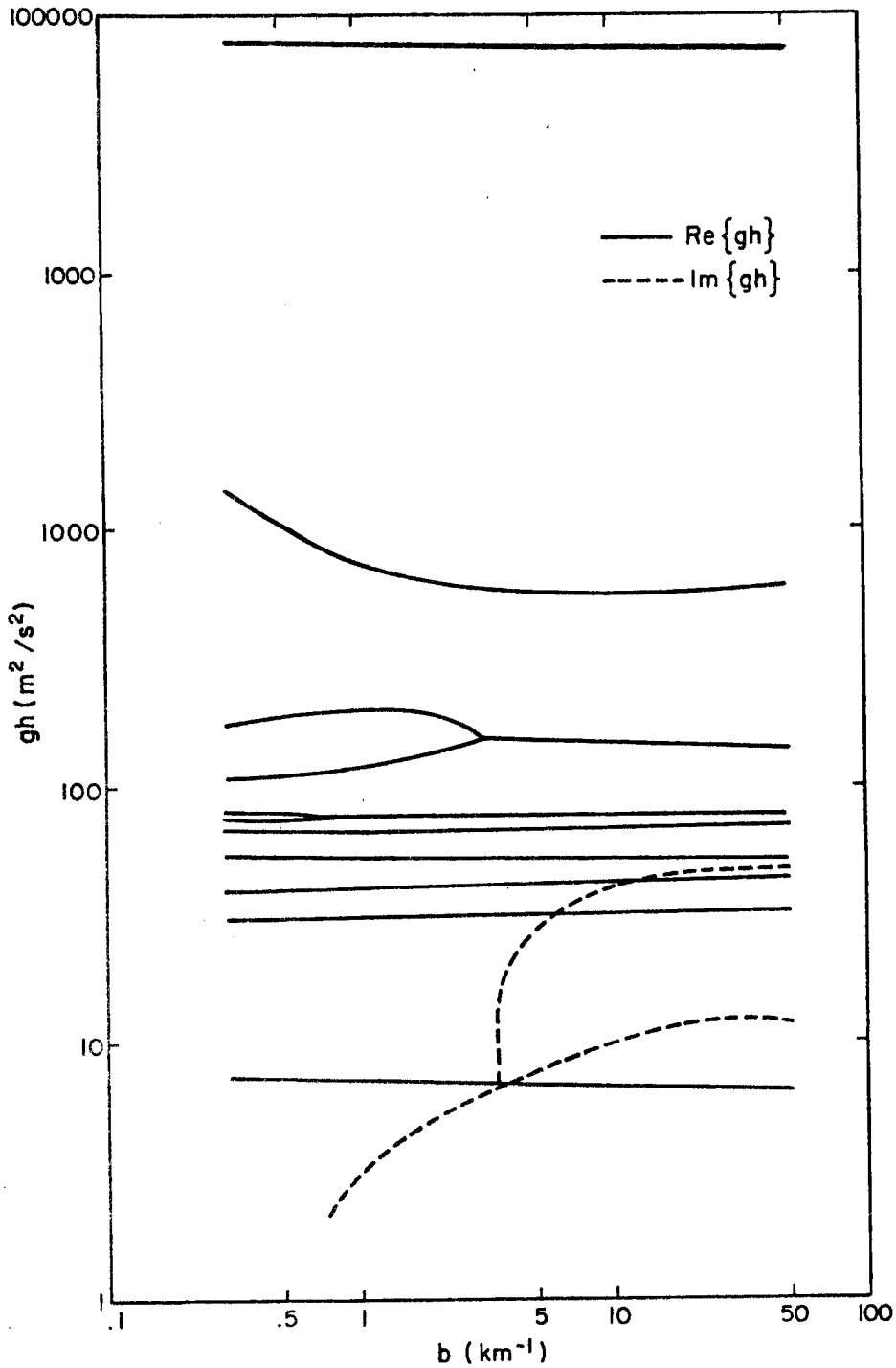

Fig. 5.13. Eigenvalues gh as a function of b.

Fig. 5.14 shows the e-folding times and phase speeds as a function of c_o for the unstable modes in Fig. 5.12. The e-folding times and phase speeds as a function of b for the unstable modes in Fig. 5.13 are shown in Fig. 5.15. Again we have chosen a gravity wave of wavelength 300 km and meridional mode n = 1. These figures are qualitatively similar to Fig. 5.6 for SL parameterization; however, there are important quantitative differences. Most noticeably, the e-folding times for the calculations with AS parameterization are much longer than those for SL parameterization. Furthermore, the phase speeds of the unstable modes are smaller for AS parameterization. We do find, as we did before, that the phase speeds of the unstable modes change relatively little compared to the changes in the e-folding times.

In Fig. 5.16 we show, for the most unstable mode in Fig. 5.15 at $b = 5\ km^{-1}$, the amplitude and phase of the vertical velocity, the cumulus heating and the adiabatic cooling. We have chosen $b = 5\ km^{-1}$ since it produces a c_o profile which agrees well with the profile given in Silva Dias and Schubert (1977). As in SL parameterization, the cumulus heating is in phase with the upward motion; however, it now shows a slight tilt with height in the upper troposphere. The amplitudes of the cumulus heating and adiabatic cooling are nearly equal. The vertical velocity has a maximum near the middle troposphere and tilts slightly with height in the upper troposphere. It is interesting to note that, although the cumulus heating profile is determined internally in the model and not specified, it still qualitatively resembles the specified profile used in SL parameterization. Amplitude and phase of the vertical velocity, cumulus heating and adiabatic cooling for the most unstable mode in Fig. 5.14 at $c_o = 2\ km^{-1}$ and at $c_o = 4\ km^{-1}$ are shown in

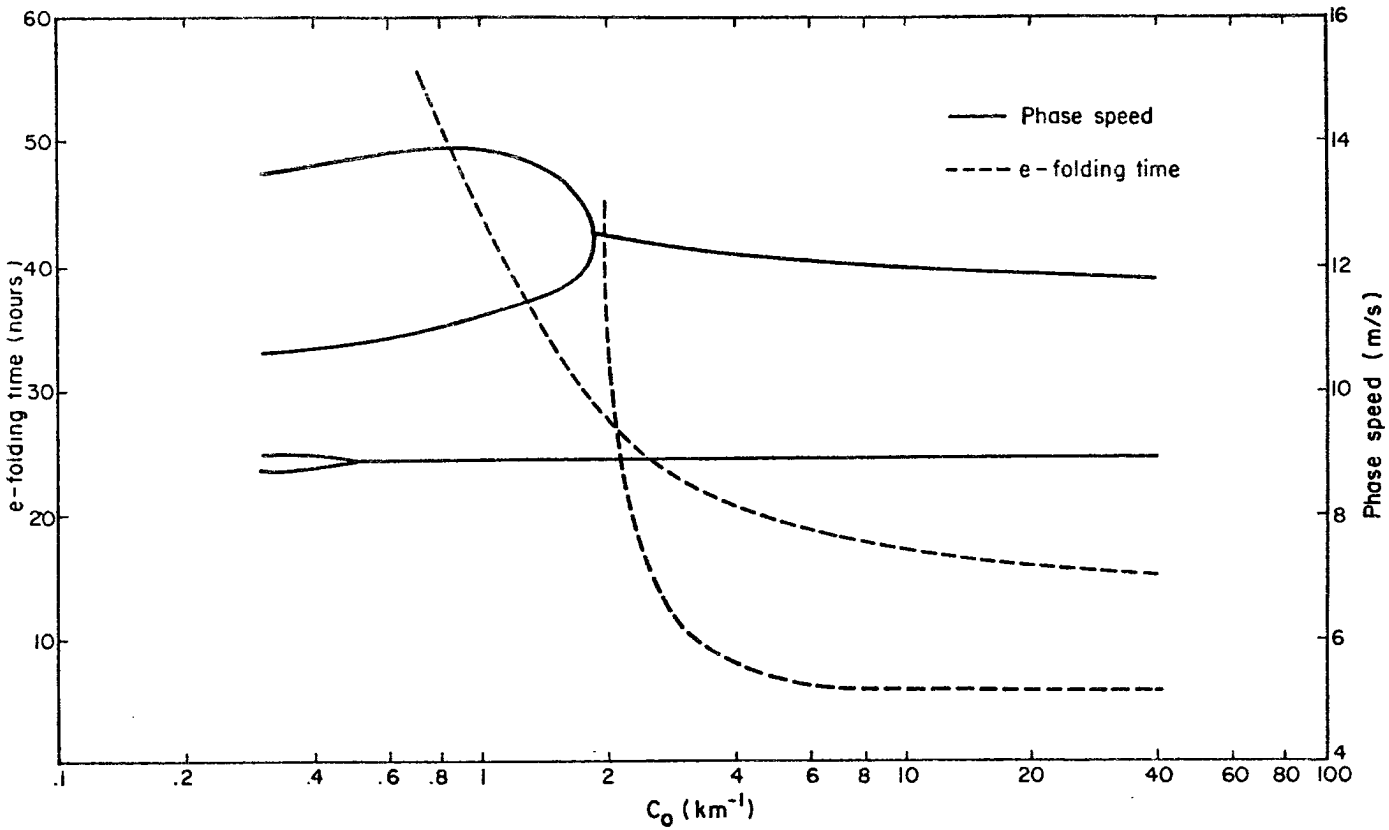

Fig. 5.14. The e-folding times and phase speeds as a function of c_0 for the unstable modes in Fig. 5.12 computed for a gravity wave of wavelength 300 km and meridional mode n = 1.

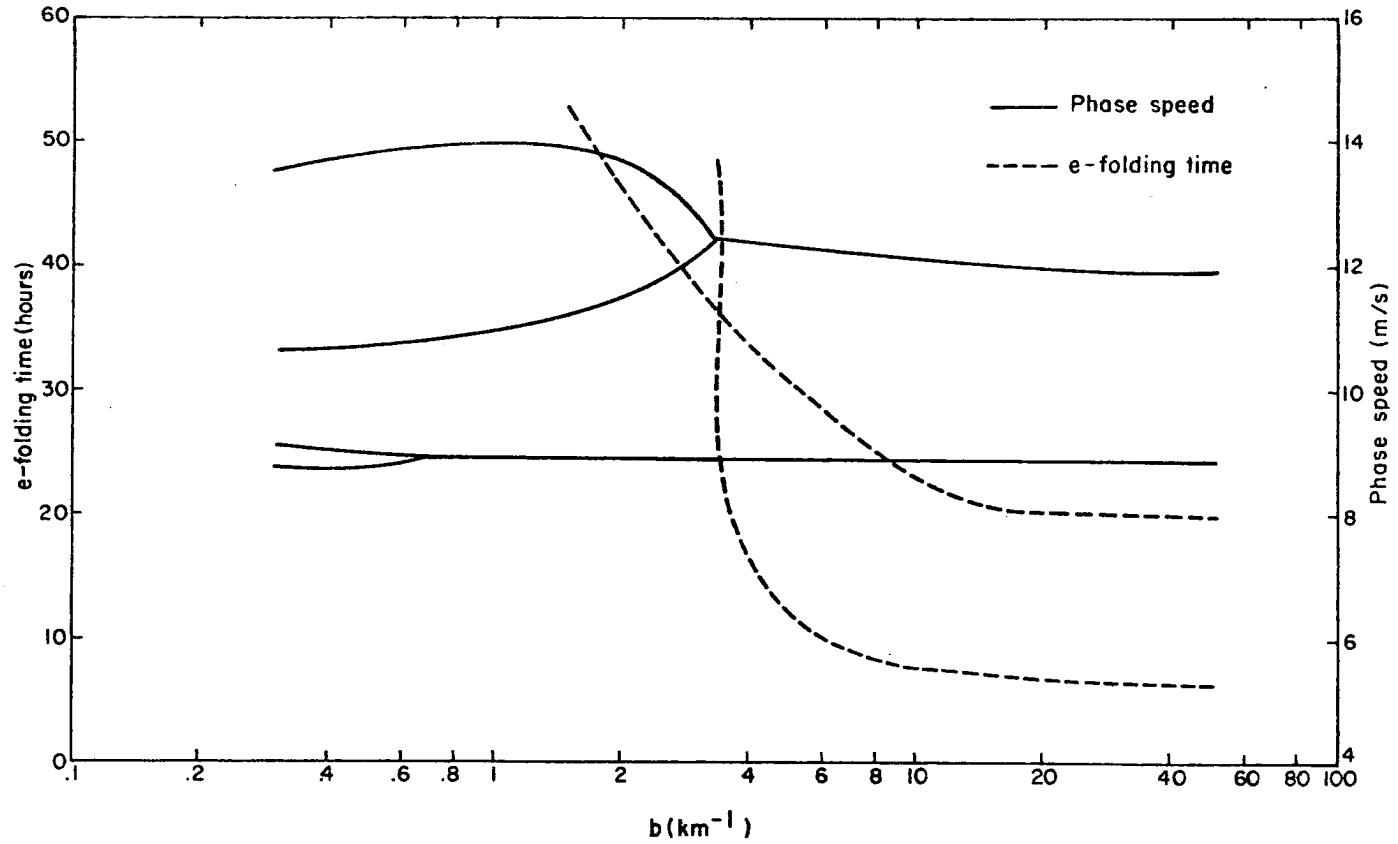

Fig. 5.15. The e-folding times and phase speeds as a function of b for the unstable modes in Fig. 5.13 computed for a gravity wave of wavelength 300 km and meridional mode n = 1.

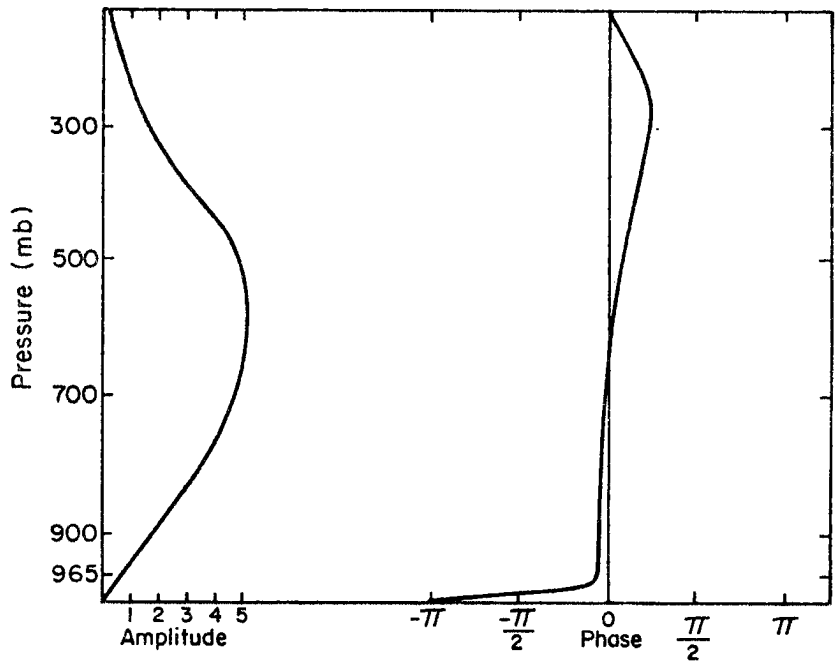

(a)

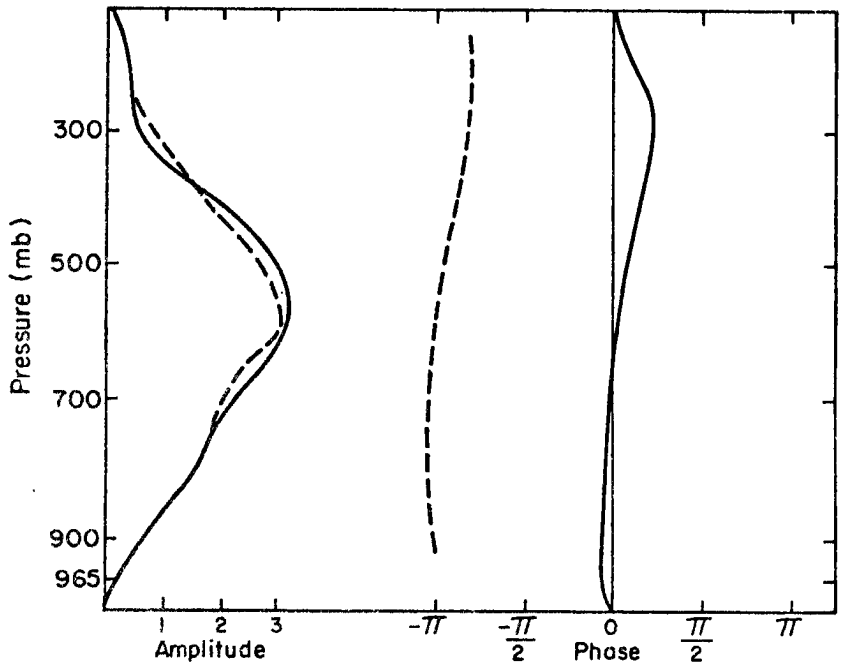

(b)

Fig. 5.16. Amplitude and phase of (a) the vertical velocity and (b) the adiabatic cooling (solid line) and cumulus heating (dashed line) for the most unstable mode in Fig. 5.15 at b = 5 km^{-1}.

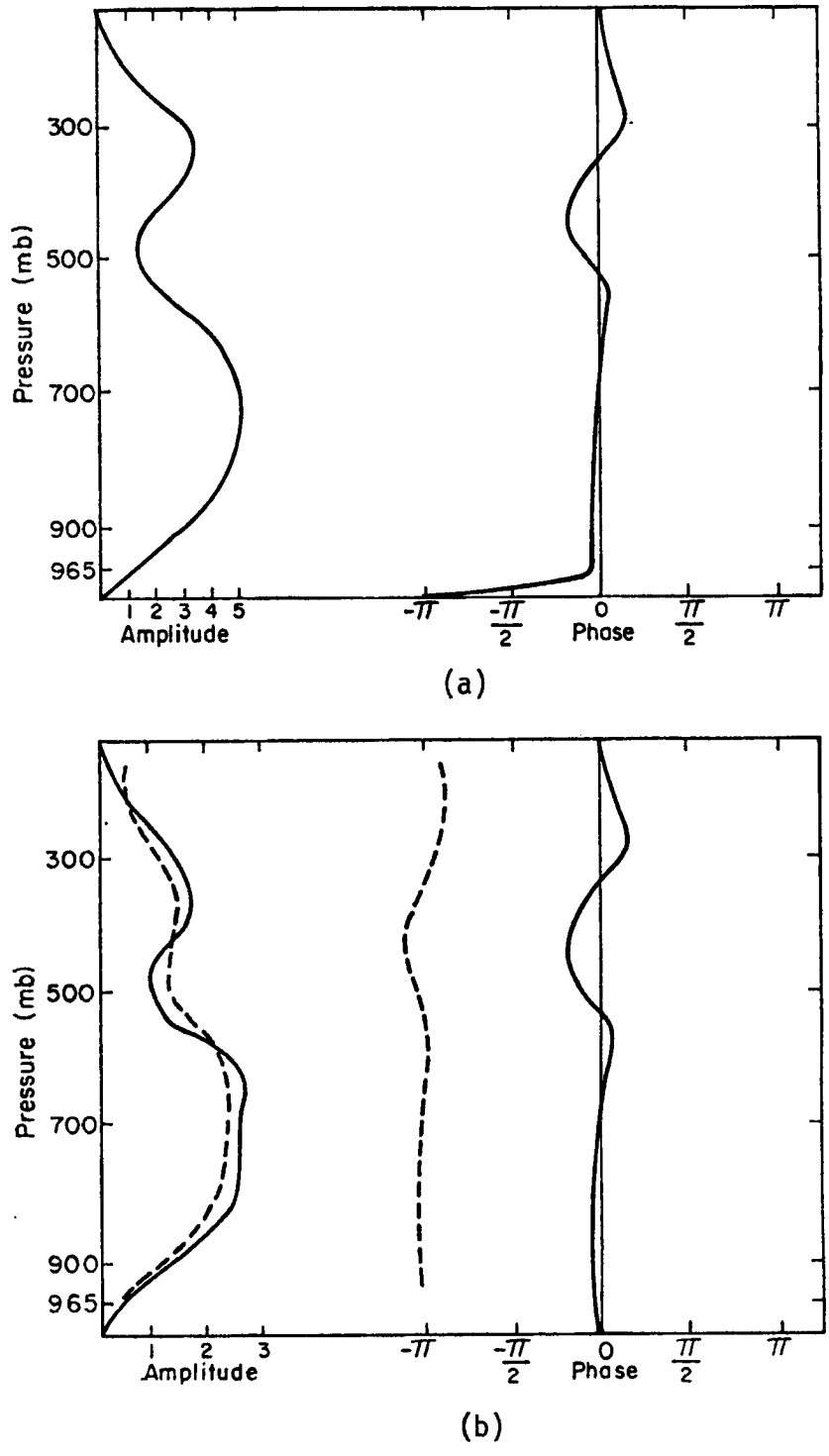

Fig. 5.17. Amplitude and phase of (a) the vertical velocity and (b) the adiabatic cooling (solid line) and cumulus heating (dashed line) for the most unstable mode in Fig. 5.14 at $c_0 = 2\ km^{-1}$.

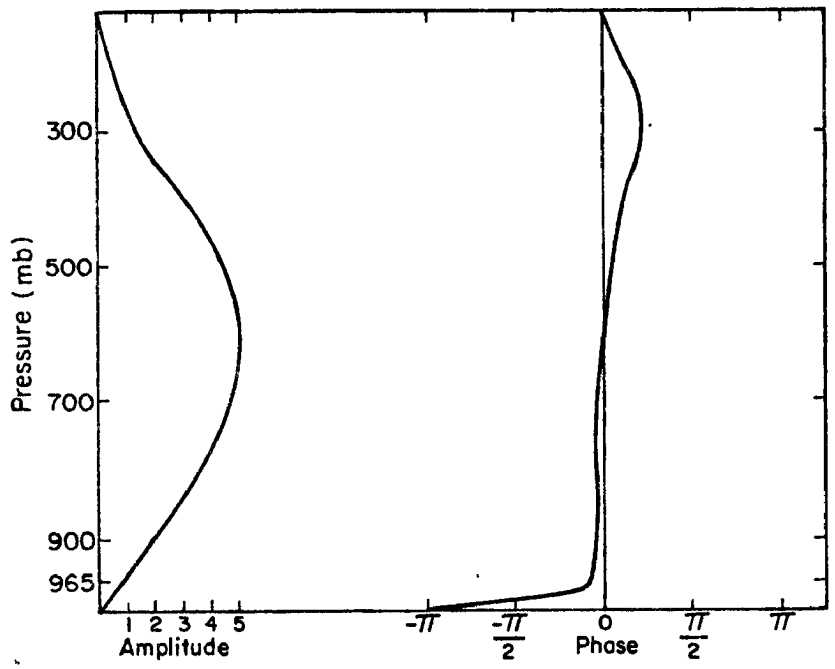

(a)

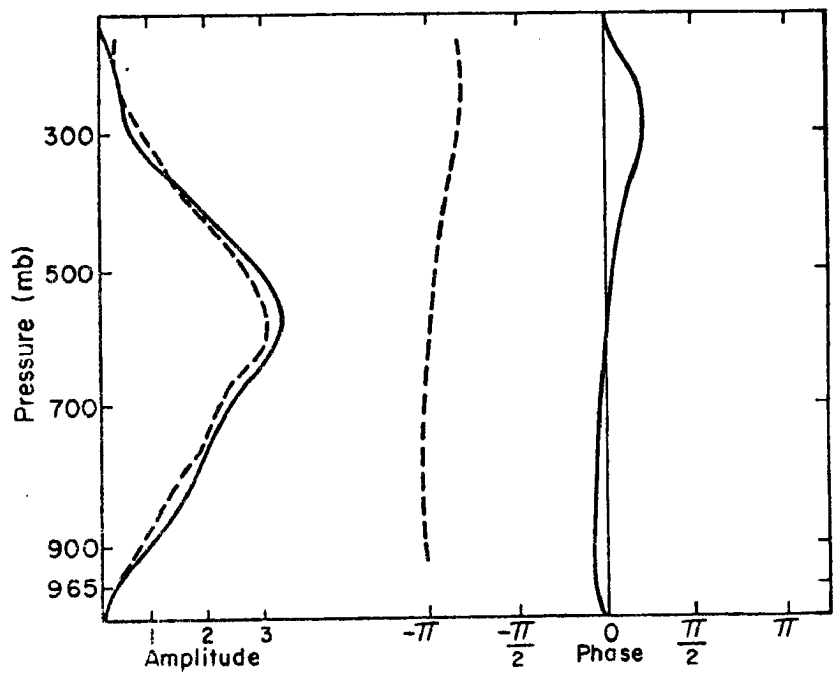

(b)

Fig. 5.18. Same as Fig. 5.17 except for $c_o = 4$ km^{-1}.

Fig. 5.17 and Fig. 5.18. Although it is not clear what a reasonable choice for c_o should be, the two values chosen above seem to lie within the range of quoted values. When $c_o = 4$ km^{-1} the amplitude and phase diagrams are essentially the same as those for $b = 5$ km^{-1}. For $c_o = 2$ km^{-1}, however, the vertical velocity exhibits two relative maximums instead of one and the cumulus heating, which is again nearly equal in amplitude to the adiabatic cooling, is no longer qualitatively similar to the cumulus heating profile specified in SL parameterization. These differences may be explained from Fig. 5.14 by noting that the most unstable mode at $c_o = 2$ km^{-1} is not the same mode as the most unstable mode at $c_o = 4$ km^{-1}.

We have, so far, presented phase speeds and e-folding times only for a particular horizontal wavelength and a particular meridional mode. For any given value of gh, we may plot the phase speed and e-folding time of several meridional modes as a function of wavelength for every wave type possible on an equatorial beta-plane. Such plots are shown in Fig. 5.19 and Fig. 5.20. We are primarily interested in the gravity modes which are the modes with the highest phase speeds and lowest e-folding times. For a complete discussion of the wave types possible on an equatorial beta-plane, the reader is referred to Matsuno (1966). We note here that for gravity waves the instability is always greatest at the shortest wavelengths. A discussion of this point and a summary of the results are contained in the final chapter.

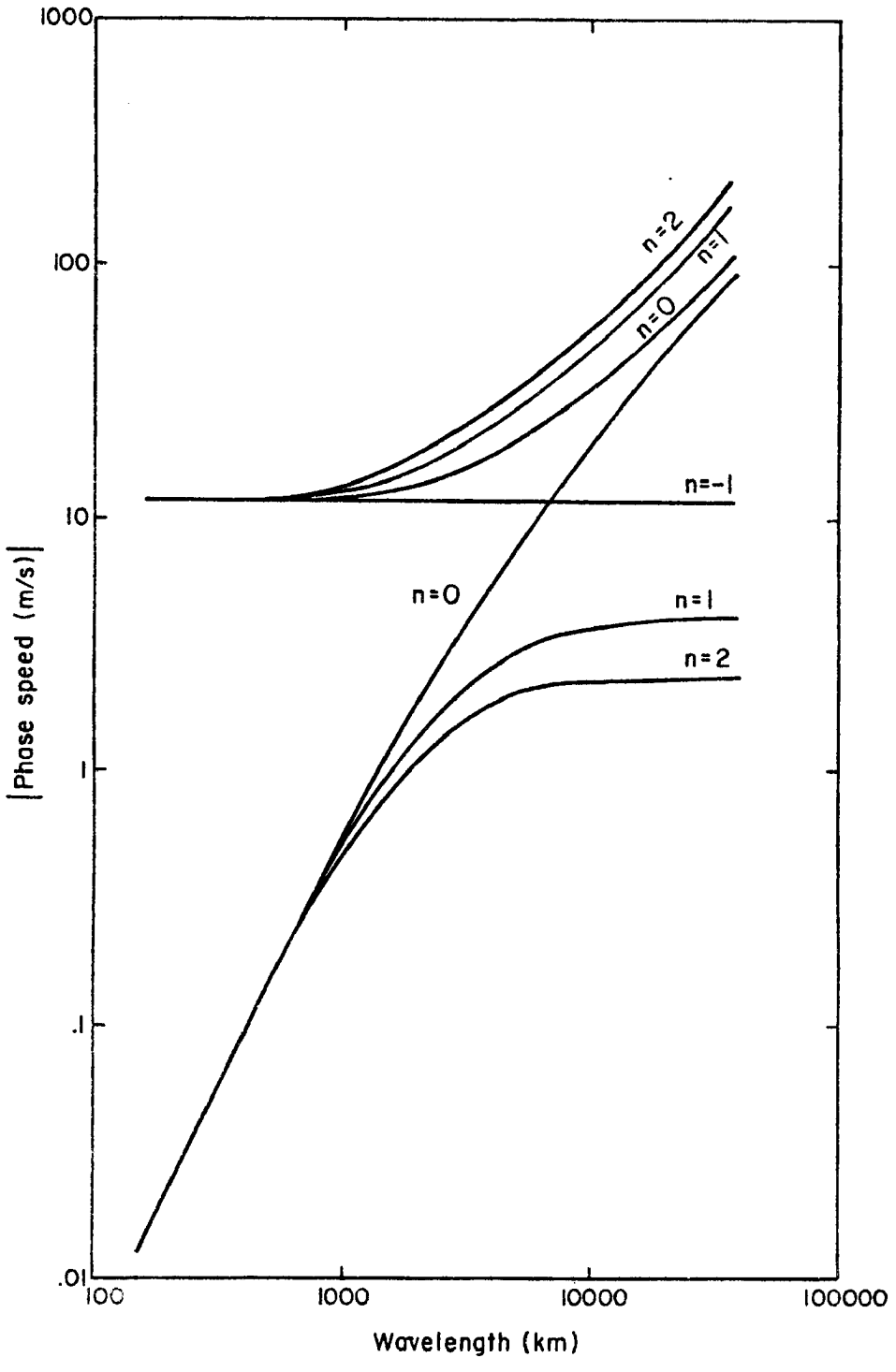

Fig. 5.19. The magnitude of the phase speed as a function of wavelength for several meridional modes n and for all wave types possible on an equatorial beta-plane. Here gh = 146.3 + 27.3i m^2/s^2.

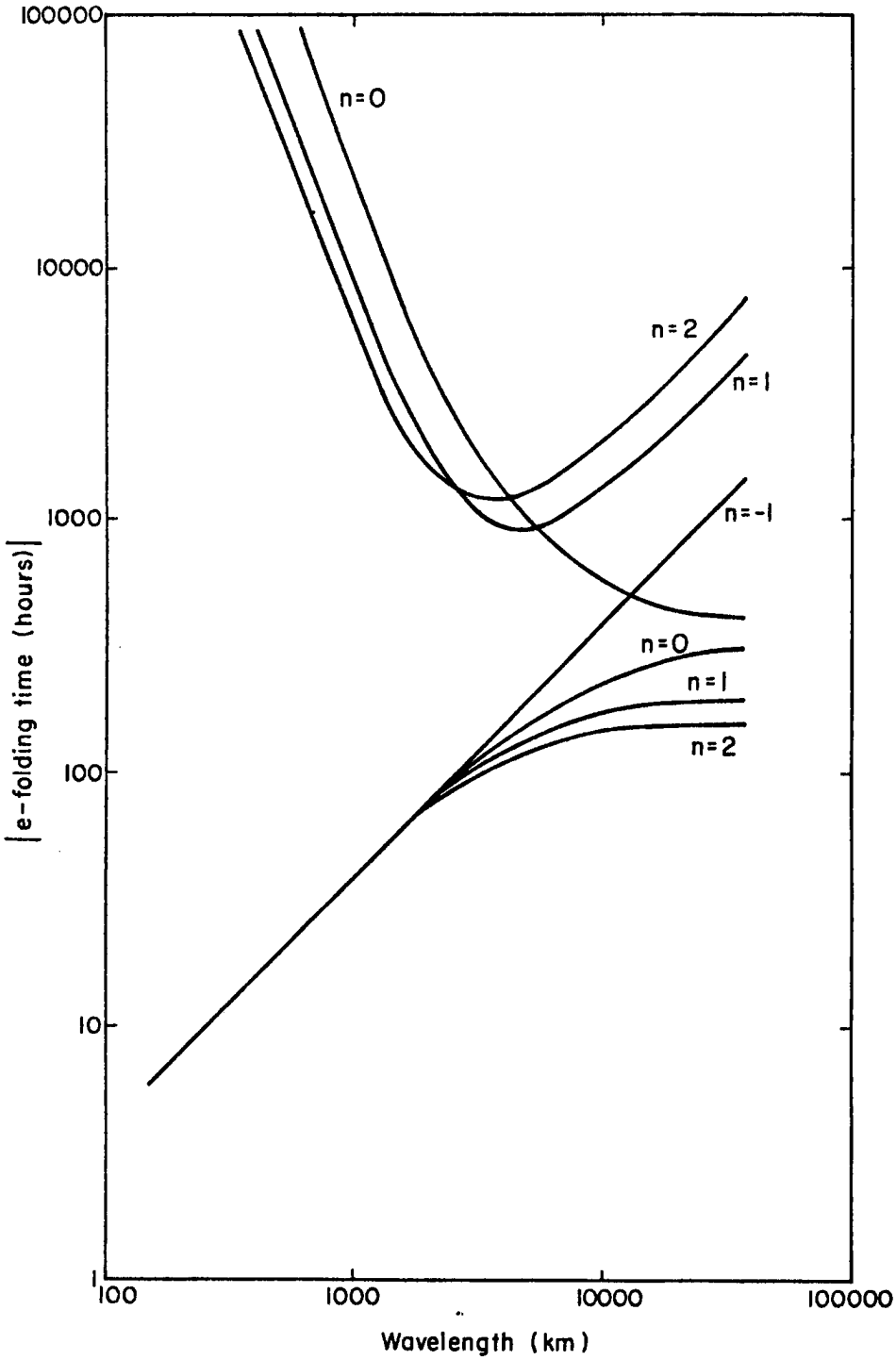

Fig. 5.20. Same as Fig. 5.19 except for the magnitude of the e-folding time as a function of wavelength.

6. SUMMARY AND CONCLUSIONS

A linear model of wave-CISK is used to compare the relatively simple parameterization scheme developed by Stevens and Lindzen with the relatively complex one developed by Arakawa and Schubert.

Chapter 2 considers the large-scale governing equations. These equations, which are formulated on an equatorial beta-plane, are linearized about a resting basic state and the dependent variables and diabatic heating are expanded in a Fourier series. The vertical structure equation and its boundary conditions are then derived along with the dispersion relation for an equatorial beta-plane.

Chapter 3 considers the governing equations for both parameterization schemes. Stevens and Lindzen parameterization is slightly modified to allow for a more realistic moisture profile. Several simplifications are made to Arakawa and Schubert parameterization in order to make the problem more tractable. In addition, the parameterization is reformulated so that the spectral parameter is the detrainment level pressure rather than the fractional rate of entrainment.

Chapter 4 considers the discrete forms of the vertical structure problem and the parameterizations. It is shown that once the heating is parameterized in terms of the vertical velocity, the vertical structure problem may be solved as a generalized matrix eigenvalue problem. The eigenvalues are used with the dispersion relation to determine the growth rates and phase speeds and the eigenvectors are used to determine the vertical structure.

The results presented in Chapter 5 are now summarized. When we looked at the eigenvalues for AS parameterization as a function of the autoconversion coefficient and at the eigenvalues of SL parameterization as a function of mixing ratio, we found that the patterns were similar; however, the eigenvalues of the unstable modes for AS parameterization had smaller real and imaginary parts than those for SL parameterization and the first internal mode became unstable for SL parameterization but not for AS parameterization. We also found that, for a given wavelength and meridional mode, the e-folding times and phase speeds of the unstable modes with AS parameterization were smaller than those for SL parameterization. Comparison of the vertical structure of the unstable modes showed that the cumulus heating was always in phase with the upward vertical motion, but was more nearly balanced by the adiabatic cooling for AS parameterization than for SL parameterization. Furthermore, the cumulus heating profile for AS parameterization, which is determined internally in the model, was remarkably similar to the specified profile used in SL parameterization. We conclude that, although there is some qualitative similarity between AS and SL parameterization, there are notable quantitative differences. Numerical modellers who use cumulus parameterization schemes should be aware of these differences.

There are several shortcomings in the model. First, a mean wind has not been included. Second, the process of momentum mixing by cumulus clouds, which was shown by Stevens, et al. (1977) to be important, has been neglected. Third, since the mean heating is zero, negative perturbation heating corresponds to negative total heating which is physically unreasonable. This negative heating is a characteristic of many wave-CISK studies and its effect on the results is not clear. In addition to these shortcomings, there is the problem that the shortest

wavelength gravity waves are the most unstable which implies that at short wavelengths, CISK degenerates into CIFK (Conditional Instability of the First Kind). If we reason as follows, this problem may not seem so serious. By definition, cumulus parameterization describes the interaction between the cumulus-scale, which is not explicitly resolved, and some specified large-scale. If we allow our specified large-scale to become so small that it approaches the cumulus-scale, then we are, at least in theory, resolving the cumulus-scale and the concept of cumulus parameterization becomes invalid. Therefore, even though the shortest wavelengths will be the most unstable, our large-scale is limited in how small it may become by the very definition of cumulus parameterization.

REFERENCES

Arakawa, A. and W.H. Schubert, 1974: Interaction of a cumulus cloud ensemble with the large-scale environment. Part I. J. Atmos. Sci., 31, 674-701.

Chang, C.-P., 1976: Vertical structure of tropical waves maintained by internally-induced cumulus heating. J. Atmos. Sci., 33, 729-739.

Charney, J.G., and A. Eliassen, 1964: On the growth of the hurricane depression. J. Atmos. Sci., 21, 68-74.

Davies, H.C., 1980: An ubiquitous property of simple wave-CISK models and its implications. J. Atmos. Sci., 37, 1437-1446.

Hack, J.J., 1977: Numerical experiments with an axisymmetric tropical cyclone model. Thesis, Department of Atmospheric Science, Colorado State University, Fort Collins, Colorado.

Hayashi, Y., 1970: A theory of large-scale equatorial waves generated by condensation heat and accelerating the zonal wind. J. Meteor. Soc. Japan, 48, 140-160.

Kuo, H.-L., 1975: Instability theory of large-scale disturbances in the tropics. J. Atmos. Sci., 32, 2229-2245.

Lindzen, R.S., 1967: Planetary waves on beta-planes. Mon. Wea. Rev., 95, 441-451.

Lindzen, R.S., 1974: Wave-CISK in the tropics. J. Atmos. Sci., 31, 156-179.

Matsuno, T., 1966: Quasi-geostrophic motions in the equatorial area. J. Meteor. Soc. Japan, 44, 25-43.

Ooyama, K., 1964: A dynamical model for the study of tropical cyclone development. Geofisica Internacional, 4, 187-198.

Schubert, W.H., 1974: Cumulus parameterization theory in terms of feedback and control. Atmospheric Science Paper No. 226, Department of Atmospheric Science, Colorado State University, Fort Collins, Colorado, 19 pp.

Silva Dias, P.L., and W.H. Schubert, 1977: Experiments with a spectral cumulus parameterization theory. Atmospheric Science Paper No. 275, Department of Atmospheric Science, Colorado State University, Fort Collins, Colorado, 132 pp.

Stark, T.E., 1976: Wave-CISK and cumulus parameterization. J. Atmos. Sci., 33, 2383-2391.

Stevens, D.E. and R.S. Lindzen, 1978: Tropical Wave-CISK with a moisture budget and cumulus friction. J. Atmos. Sci., 35, 940-961.

Stevens, D.E., R.S. Lindzen and L.J. Shapiro, 1977: A new model of tropical waves incorporating momentum mixing by cumulus convection. Dyn. Atmos. Oceans, 1, 365-425.

Wada, M., 1977: The properties of typhoon-scale disturbances produced by Arakawa-Schubert parameterization. J. Meteor. Soc. Japan, 55, 364-391.

APPENDIX A

PRINCIPAL SYMBOLS

A	cloud work function
C	condensation
E	evaporation
F	large-scale forcing term in Fredholm integral equation
F_s, F_h, F_ℓ	convective scale fluxes of dry static energy, moist static energy, and liquid water
J	vertical structure of perturbation diabatic heating
$K, \bar{K}$	kernel of Fredholm integral equation: total, basic state
L	latent heat of vaporization
$P, \bar{P}, P'$	precipitation: total, basic state, perturbation
$Q, \bar{Q}, Q'$	diabatic heating: total, basic state, perturbation
R	gas constant for dry air or convective scale sink of liquid water (rain)
$T, \bar{T}, T'$	temperature (absolute): total, basic state, perturbation
W	vertical structure of perturbation vertical velocity
Y	horizontal (y) structure of perturbation diabatic heating and perturbation vertical velocity
a, b, c	parameters used in determining autoconversion coefficient profile
c_o	autoconversion coefficient
c_p	specific heat at constant pressure for dry air
f	coriolis parameter

g	acceleration due to gravity
$h,\bar{h}$	equivalent depth or moist static energy: total, basic state
$h^*,\bar{h}^*$	saturation mixing ratio: total, basic state
$h_c,\bar{h}_c$	cloud moist static energy: total, basic state
h_M	mixed layer moist static energy
k	horizontal (x) wavenumber
$\ell,\bar{\ell}$	cloud liquid water content: total, basic state
$m_B,\bar{m}_B,m'_B$	mass flux distribution function: total, basic state, perturbation
n	Fourier summation index, meridional and vertical mode number
p	pressure
$\hat{p}$	detrainment pressure
p_{00}	fixed surface pressure
p_T	model top pressure
p_B	mixed layer top pressure
p_{CT}	upper boundary of heated region for Stevens and Lindzen parameterization
p_a,p_d	parameters for moisture profile used in Stevens and Lindzen parameterization
$q,\bar{q}$	mixing ratio: total, basic state
$q^*,\bar{q}^*$	saturation mixing ratio: total, basic state
$q_c,\bar{q}_c$	cloud mixing ratio: total, basic state
q_M	mixed layer mixing ratio
q_a	moisture parameter for Stevens and Lindzen parameterization
$r,\bar{r}$	rain distribution function: total, basic state
$s,\bar{s}$	dry static energy: total, basic state
$s_c,\bar{s}_c$	cloud dry static energy: total basic state

t	time
$u,v,\bar{u},\bar{v},u',v'$	horizontal velocities: total, basic state, perturbation
$\underset{\sim}{v}$	horizontal velocity vector
w	vertical velocity in z-coordinates
x,y	horizontal positions
$z,\bar{z}$	geopotential height: total, basic state
z^*	log-pressure vertical coordinate
Γ	static stability in log-pressure coordinates
α	magnitude of cumulus heating in Stevens and Lindzen parameterization
β	$= df/dy$
γ	$= \frac{L}{c_p} \left(\frac{\partial q^*}{\partial T}\right)_p$
δ	exponential rate of moisture decrease with pressure in Stevens and Lindzen parameterization
$\eta,\bar{\eta}$	normalized cloud mass flux: total, basic state
κ	$= R/c_p$
$\lambda,\bar{\lambda}$	fractional entrainment rate: total, basic state
σ	complex wave frequency
$\phi,\bar{\phi},\phi'$	geopotential: total, basic state, perturbation
$\omega,\bar{\omega},\omega'$	vertical velocity in p-coordinates: total, basic state, perturbation

APPENDIX B

DETERMINATION OF THE SATURATION MIXING RATIO AND GAMMA

Teton's formula for the saturation mixing ratio e_s is

$$e_s = 610.78 \exp\left[\frac{a(T-273.16)}{T-b}\right], \tag{B1}$$

where e_s is in units of Pa, T is in units of degrees Kelvin, a = 17.269 and b = 35.86 K. Once e_s is determined, q^* may be obtained from

$$q^* = 0.622 \frac{e_s}{p-e_s} . \tag{B2}$$

Using (B1), (B2) and the definition of γ given in (3.24), we may write

$$\gamma = 4098.3 \frac{L}{c_p} \frac{p}{p-e_s} \frac{q^*}{(T-b)^2} . \tag{B3}$$

APPENDIX C

THE DISCRETE FORM OF THE FREDHOLM INTEGRAL EQUATION

We begin the derivation of the Fredholm integral equation (3.28) by writing the discrete moist static energy budget in the form

$$\eta(k-1,n)h_c(k-1,n) = h_M + \sum_{k'=k}^{K-2} h(k')[\eta(k'-1,n)-\eta(k'+1,n)]. \qquad (C1)$$

Here, and in all summations that follow, the summation index takes on only even values. Substituting (C1) into the discrete form of the cloud work function (4.28) we find

$$\begin{aligned} A(n) = \sum_{k'=n}^{K-2} \beta(k') \Big\{ & (\Delta p^-(k')+\Delta p^+(k'))h_M \\ & + (\Delta p^-(k')+\Delta p^+(k')) \sum_{k''=k'+2}^{K-2} h(k'')[\eta(k''-1,n)-\eta(k''+1,n)] \\ & + \Delta p^-(k')h(k')[\eta(k'-1,n)-\eta(k'+1,n)] \\ & - h^*(k')[\eta(k'-1,n)\Delta p^-(k')+\eta(k'+1,n)\Delta p^+(k')] \Big\} . \qquad (C2) \end{aligned}$$

We now apply the quasi-equilibrium assumption and set the time derivative of A(n) equal to zero. Time changes in β are neglected. The terms in the resulting equation are divided into two types: those directly involving the time derivatives of large-scale quantities and those involving the time derivatives of η. The quasi-equilibrium assumption may thus be written

$$\sum_{k'=n}^{K-2} \beta(k') \Big\{(\Delta p^-(k')+\Delta p^+(k')) \sum_{k''=k'+2}^{K-2} [\eta(k''-1,n)-\eta(k''+1,n)] \frac{\partial h(k'')}{\partial t}$$

$$+ \Delta p^-(k')[\eta(k'-1,n)-\eta(k'+1,n)]\frac{\partial h(k')}{\partial t}$$

$$- [\eta(k'-1,n)\Delta p^-(k')+\eta(k'+1,n)\Delta p^+(k')] \frac{\partial h^*(k')}{\partial t}\Big\}$$

$$+ \sum_{k'=n}^{K-2} \beta(k') \Big\{(\Delta p^-(k')+\Delta p^+(k'))$$

$$\times \sum_{k''=k'+2}^{K-2} h(k'')[\frac{\partial \eta(k''-1,n)}{\partial t} - \frac{\partial \eta(k''+1,n)}{\partial t}]$$

$$+ \Delta p^-(k')h(k')[\frac{\partial \eta(k'-1,n)}{\partial t} - \frac{\partial \eta(k'+1,n)}{\partial t}]$$

$$- h^*(k')[\Delta p^-(k') \frac{\partial \eta(k'-1,n)}{\partial t}+\Delta p^+(k') \frac{\partial \eta(k'+1,n)}{\partial t}]\Big\} = 0. \qquad \text{(C3)}$$

The time derivative of h* may be written

$$\frac{\partial h^*(k')}{\partial t} = (1+\gamma(k')) \frac{\partial s(k')}{\partial t} , \qquad \text{(C4)}$$

and (4.14) may be used to write the time derivative of η as

$$\frac{\partial \eta(k-1,n)}{\partial t} = (p_B-p(k-1))\eta(k+1,n) \frac{\partial \lambda(n)}{\partial t}. \qquad \text{(C5)}$$

Using (C4), (C5) and the discrete large-scale budgets of s and h (4.23) and (4.24), we may rewrite (C3) as

$$\sum_{k'=n}^{K-2} \beta(k') \Big\{ (\Delta p^-(k')+\Delta p^+(k')) \sum_{k''=k'+2}^{K-2} [\eta(k''-1,n)-\eta(k''+1,n)]\frac{\partial h(k')}{\partial t}\Big|_{LS}$$

$$+ \Delta p^-(k')[\eta(k'-1,n)-\eta(k'+1,n)] \frac{\partial h(k')}{\partial t}\Big|_{LS}$$

$$- [\eta(k'-1,n)\Delta p^-(k')+\eta(k'+1,n)\Delta p^+(k')](1+\gamma(k')) \frac{\partial s(k')}{\partial t}\Big|_{LS}\Big\}$$

$$+ \sum_{n'=n_{min}}^{K-4} \left\{ \sum_{k'=n}^{K-2} \beta(k') \left\{ (\Delta p^-(k') + \Delta p^+(k')) \frac{g}{\Delta p} \right.\right.$$

$$\times \sum_{k''=k'+2}^{K-2} [\eta(k''-1,n) - \eta(k''+1,n)][F_h(k''+1,n') - F_h(k''-1,n')]$$

$$+ \Delta p^-(k')[\eta(k'-1,n) - \eta(k'+1,n)][F_h(k'+1,n') - F_h(k'-1,n')] \frac{g}{\Delta p}$$

$$- [\eta(k'-1,n)\Delta p^-(k') + \eta(k'+1,n)\Delta p^+(k')] (1+\gamma(k'))$$

$$\times \left[\frac{g}{\Delta p} [F_{s-L\ell}(k'+1,n') - F_{s-L\ell}(k'-1,n')] \right.$$

$$\left.\left.\left. + Lg\eta(k'+1,n')c_o(k',n')\ell(k'-1,n') \right] \right\} \right\} M_B(n')$$

$$+ \sum_{k'=n}^{K-2} \beta(k') \left\{ (\Delta p^-(k') + \Delta p^+(k')) \sum_{k''=k'+2}^{K-2} h(k'')[(p_B - p(k''-1))\eta(k''+1,n) \right.$$

$$- (p_B - p(k''+1))\eta(k''+3,n)] + \Delta p^-(k')h(k')[(p_B - p(k'-1))\eta(k'+1,n)$$

$$- (p_B - p(k'+1))\eta(k'+3,n)] - h^*(k')[\Delta p^-(k')(p_B - p(k'-1))\eta(k'+1,n)$$

$$\left. + \Delta p^+(k')(p_B - p(k'+1))\eta(k'+3,n)] \right\} \frac{\partial \lambda(n)}{\partial t} = 0. \qquad \text{(C6)}$$

Here

$$F_h(k'-1,n) = \eta(k'-1,n)\,[h_c(k'-1,n) - h(k'-1)], \qquad \text{(C7)}$$

$$F_{s-L\ell}(k'-1,n) = \eta(k'-1,n)[s_c(k'-1,n) - s(k'-1) - L\ell(k'-1,n)]. \qquad \text{(C8)}$$

Note that the terms have been divided into three types: those involving the large-scale advection, those involving the cloud base mass flux M_B and those involving the time derivatives of λ. If we let the first term be denoted by $F_1(n)$, everything inside the outermost brackets in the

second term be denoted by $K_1(n,n')$ and everything in the third term multiplying $\partial\lambda(n)/\partial t$ be denoted by $\partial A(n)/\partial\lambda$ we may write

$$F_1(n) + \sum_{n'=n_{min}}^{K-4} K_1(n,n')M_B(n') + \frac{\partial A(n)}{\partial\lambda}\frac{\partial\lambda(n)}{\partial t} = 0. \qquad (C9)$$

An expression for $\partial\lambda(n)/\partial t$ may be derived from the cloud top condition

$$\eta(n,n)h^*(n) = \eta(n,n)h_c(n,n), \qquad (C10)$$

which may be rewritten

$$\eta(n,n)h^*(n) = h_M + \lambda(n)\Delta p \sum_{k'=n+2}^{K-2} h(k')\eta(k'+1,n) + \tfrac{1}{2}\, h(n)\lambda(n)\Delta p\eta(n+1,n). \qquad (C11)$$

Taking the time derivative of (C11) we may show, after some considerable manipulation, that

$$\frac{\partial\lambda(n)}{\partial t} = \frac{1}{f(n)}\left\{\lambda(n)\Delta p \sum_{k'=n+2}^{K-2} \eta(k'+1,n)\left.\frac{\partial h(k')}{\partial t}\right|_{LS} + \tfrac{1}{2}\lambda(n)\Delta p\eta(n+1,n)\left.\frac{\partial h(n)}{\partial t}\right|_{LS} - \eta(n,n)(1+\gamma(n)\left.\frac{\partial s(n)}{\partial t}\right|_{LS}\right\}$$

$$+ \sum_{n'=n_{min}}^{K-4} \frac{1}{f(n)}\left\{\lambda(n)g \sum_{k'=n+2}^{K-2} \eta(k'+1,n)[F_h(k'+1,n')-F_h(k'-1,n')] + \tfrac{1}{2}\lambda(n)g\eta(n+1,n)[F_h(n+1,n')-F_h(n-1,n')] - \eta(n,n)(1+\gamma(n))\left[\frac{g}{\Delta p}[F_{s-L\ell}(n+1,n')-F_{s-L\ell}(n-1,n')] + Lg\eta(n+1,n')c_o(n,n')\ell(n-1,n')\right]\right\} M_B(n') \qquad (C12)$$

where

$$f(n) = \Delta p\left\{h^*(n)[\tfrac{1}{2}\eta(n+1,n)+(\tfrac{K-n}{2}-1)\eta(n+3,n)(1+\lambda(n)\tfrac{\Delta p}{2})]\right.$$

$$-\lambda(n)\Delta p \sum_{k'=n+2}^{K-2} h(k')\left(\frac{K-k'}{2} - 1\right)\eta(k'+3,n)$$

$$- \tfrac{1}{2}\lambda(n)h(n)\left(\frac{K-n}{2} - 1\right)\Delta p\eta(n+3,n)$$

$$\left. - \sum_{k'=n+2}^{K-2} h(k')\eta(k'+1,n) - \tfrac{1}{2}h(n)\eta(n+1,n)\right\} . \qquad \text{(C13)}$$

Here again we note that the terms in (C12) are of two types: those which depend on the large-scale advection and those which depend on the cloud base mass flux M_B. If we let the product of $\partial A(n)/\partial\lambda$ with the first term be denoted by $F_2(n)$, and the product of $\partial A(n)/\partial\lambda$ with everything inside the outermost summation in the second term be denoted by $K_2(n,n')$ we may write (C9) as

$$F_1(n) + F_2(n) + \sum_{n'=n_{min}}^{K-4} (K_1(n,n')+K_2(n,n'))M_B(n') = 0. \qquad \text{(C14)}$$

Letting

$$F(n) = F_1(n) + F_2(n), \qquad \text{(C15)}$$

$$K(n,n') = K_1(n,n') + K_2(n,n'), \qquad \text{(C16)}$$

we have

$$\sum_{n'=n_{min}}^{K-4} K(n,n')M_B(n') + F(n) = 0 \qquad \text{(C17)}$$

which is the discrete form of the Fredholm integral equation given in the main text.